Yerbilimleri, 2024, 45 (1), 1-51, 1393877

Hacettepe Üniversitesi Yerbilimleri Uygulama ve Araştırma Merkezi Bülteni (*Bulletin of the Earth Sciences Application and Research Centre of Hacettepe University*

YERBİLİMLERİ
Bulletin for Earth Sciences

ISSN: 2687- 2978

Mineralogical, Petrographical, and Geochemical Properties of the Late Oligocene Coal Seam (Seam-VI): Insights into Elemental Enrichments and Palaeodepositional Environment (İbrice field, Thrace Basin)

Geç Oligosen Yaşlı Kömür Damarının (VI No'lu) Mineralojik, Petrografik ve Jeokimyasal Özellikleri: Elementel Zenginleşmeler ve Çökelme Ortamı Değerlendirmeleri (İbrice Sahası, Trakya Havzası)

ALİ İHSAN KARAYİĞİT [1], RIZA GÖRKEM OSKAY [2*], CÜNEYT BİRCAN [3]

[1] Hacettepe University, Department of Geological Engineering, Ankara, Türkiye

[2] Hacettepe University, Başkent OSB Technical Sciences Vocational School, Ankara, Türkiye

[3] Balıkesir University, Department of Geological Engineering, Balıkesir, Türkiye

Received *(geliş)*: 21 November (*Kasım*) 2023 Accepted *(kabul):* 26 Febuary(*Şubat*) 2024

ABSTRACT

The Thrace Basin hosts several mineable coal seams (upwards numbered I to VII) within the coal-bearing Late Oligocene-age Danişmen Formation. For the first time, the properties of the Seam-VI in the İbrice (Malkara) area have been investigated in order to evaluate elemental enrichments and palaeoenvironmental conditions. The xylite-rich and mineral-rich lithotypes were identified from the studied coal samples representing the whole-coal thickness. The coal samples, on a dry basis, display variable ash yields (13.2–63.0%), total C (21.2–57.8%), and total S (0.9–4.1%) contents. The minerals identified using XRD-whole rock analysis include clay minerals, quartz, pyrite, calcite, dolomite, and feldspars. Siderite is only identified in a single sample. Aragonite is detected in two samples, which contain fossil shell remains. The SEM observations agree with XRD data, and apatite, barite, biotite, pentlandite, sphalerite, Ti-oxide, and zircon were also identified as accessory phases. Huminite is the predominant maceral group in the studied samples, while liptinite and inertinite group macerals display variable proportions. The mean %Rr values of ulminite macerals are around 0.40-0.41±0.01-0.02%, indicating relatively low-rank coal. This study implies that the precursor peat-mires of the Seam-VI were mainly developed under forested mire conditions, where woody peat-forming plants were abundant, and occasionally the contributions of herbaceous plants were important. The coexistence of syngenetic pyrite and carbonate minerals (e.g., siderite and carbonate mineral bands) could be related to the development of weakly acidic to neutral conditions within palaeomires. Furthermore, the predominance of clay minerals and the presence of detrital accessory minerals (e.g., apatite, pentlandite, and Ti-oxides) can also be indicators of clastic influx into palaeomires. Although aluminosilicate minerals (e.g., clay minerals) are abundant in dominant phases, SEM-EDX data shows that accessory minerals mainly control the elemental enrichments in the Seam-VI. The Mn enrichments in the samples seem to be controlled by Mn-bearing siderite

micronodules. Considering the presence of sulphide mineralization and metallic ore deposits in the Strandja and Rhodope massifs, enrichments of Cr, Co, Ni, Ge, and Mo are related to As-bearing pyrite grains and accessory sphalerite and pentlandite grains within clay mineral aggregates in the samples. In addition, the Sr-bearing barite overgrowths around feldspar grains and syngenetic carbonate mineral bands could also cause Sr enrichments. Overall, clastic influx ratios into palaeomires and pH conditions during peat accumulation controlled the elemental enrichments in the Seam-VI.

Keywords: Coal, Danişmen Formation, elemental enrichments, mineralogy, petrography, Thrace Basin

ÖZ

Trakya Havzası, Geç Oligosen yaşlı, kömür içeren Danişmen Formasyonu içerisinde, I'den VII'ye kadar işletilebilir kömür damarına ev sahipliği yapmaktadır. Elementel zenginleşmelerin ve paleoortam koşullarının değerlendirilmesi amacıyla İbrice (Malkara) bölgesindeki Damar-VI'nın özellikleri ilk kez bu çalışma kapsamında araştırılmıştır. İncelenen kömür örneklerinden tüm kömür kalınlığını temsil edecek şekilde ksilitçe zengin ve mineralce zengin litotipleri tanımlanmıştır. Kömür örnekleri kuru bazda geniş bir aralıkta kül verimi (%13,2–63,0), toplam C (%21,2–57,8) ve toplam S (%0,9–4,1) içeriğini göstermektedir. XRD-tüm kaya analizi kullanılarak tanımlanan mineraller kil mineralleri, kuvars, pirit, kalsit, dolomit ve feldspatlardır. Siderit yalnızca bir örnekten tanımlanırken, fosil kabuk kalıntıları içeren iki örnekte aragonit tespit edilmiştir. SEM gözlemleri XRD verileriyle uyumlu olup, apatit, barit, biyotit, pentlandit, sfalerit, Ti-oksit ve zirkon da aksesuar fazlar olarak belirlenmiştir. Çalışılan örneklerde hüminit baskın maseral grubunu oluştururken, liptinit ve inertinit grubu maseraller değişken oranlar göstermektedir. Ulminit maserallerinin ortalama %Rr değerleri 0,40-0,41±0,01-0,02% civarında olup, nispeten düşük dereceli kömürü işaret etmektedir. Bu çalışma, Damar-VI'nın ilksel turba bataklıklarının çoğunlukla odunsu turba oluşturan bitkilerin yaygın olduğu ormanlık bataklık koşullarında geliştiğini ve zaman zaman otsu bitkilerin katkılarının arttığını işaret etmektedir. Sinjenetik pirit ve karbonat minerallerinin (örneğin, siderit ve karbonat mineral bantları) bir arada bulunması, ilksel turbalıklardaki zayıf asidik ila nötr koşulların gelişimi ile ilişkili olabilir. Ayrıca, kil minerallerinin baskınlığı ve kırıntılı aksesuar minerallerin (örneğin apatit, pentlandit ve Ti-oksitler) varlığı da ilksel turbalıklara kırıntılı sedimant girdisinin göstergeleri olabilir. Her ne kadar alüminosilikat mineralleri (örneğin kil mineralleri) baskın bol ve baskın fazlar olarak bulunsa da, SEM-EDX verileri esasen aksesuar minerallerin Damar-VI'daki elementel zenginleşmeleri kontrol ettiğini göstermektedir. Örneklerdeki Mn zenginleşmelerinin Mn içeren siderit mikronodüller tarafından kontrol edildiği görülmektedir. Istranca ve Rodop masiflerinde sülfit mineralizasyonu ve metalik cevher yataklarının varlığı göz önüne alındığında, örneklerdeki Cr, Co, Ni, Ge ve Mo zenginleşmeleri, kil mineral agregatları içindeki As içeren pirit taneleri ve aksesuar sfalerit ve pentlandit taneleri ile ilişkilidir. Ayrıca feldspat taneleri etrafındaki Sr taşıyan barit büyümeleri ve sinjenetik karbonat mineral bantları Sr zenginleşmesine neden olabilir. Genel olarak, turba birikimi sırasında ilksel turbalıklara kırıntı girdisinin oranı ve pH koşullarının Damar-VI'daki element zenginleşmelerini kontrol ettiği anlaşılmaktadır.

Anahtar Kelimeler: *Kömür, Danişmen Formasyonu, element zenginleşmesi, mineraloji, petrografi, Trakya Havzası*

https://doi.org/10.17824/yerbilimleri.1393877

*Sorumlu Yazar/ Corresponding Author: rizagorkemoskay@hacettepe.edu.tr

INTRODUCTION

With increasing energy demands, elemental and mineralogical features of coal seams became important for reducing environmental impacts, recovering some critical elements from coal and its combustion remains, and improving the combustion efficiency of boilers in power plants (e.g., Dai and Finkelman, 2018; Dai et al., 2021, 2023; Finkelman et al., 2019;

Hower et al., 2023; Pan et al., 2020). Besides, mineralogical, petrographic, and geochemical properties of coal seams could provide essential data about the palaeodepositional conditions during the precursor peat accumulation. For instance, predominance of syngenetic carbonate minerals and natural zeolite minerals in coal seams could indicate alkaline conditions within the palaeomire, while the presence of syngenetic authigenic kaolinite could be evidence of open hydrogeological conditions and synchronous and/or epiclastic volcanic inputs into palaeomires (e.g., Dai et al., 2020a; Karayiğit et al., 2017; Querol et al., 1997; Ward, 2002, 2016). Furthermore, relatively high concentrations of B, S, and/or Mn could indicate possible marine influence into palaeomires (e.g., Dai et al., 2020a; Goodarzi and Swaine, 1994; Hower et al., 2002). Therefore, several studies have been conducted on coal deposits across the world, as well as on Turkish coal deposits within this scope. The studies about Turkish coal seams are mostly focused on Neogene coal seams due to their usages as a feeding coal-fired power plants (e.g., Gürdal, 2011; Karayiğit et al., 2000; Palmer et al., 2004). Even though most coal resources in the Thrace Basin are hosted in the Oligocene sequences, these seams received less concerns than the Turkish Neogene coals, and a limited number of studies focused on these seams (e.g., Çelik et al., 2017; Erarslan and Örgün, 2017; Erarslan et al., 2014, 2020).

The Thrace Basin is bordered by the Strandja Massif to the north, the Rhodope Massif to the west, and the Sakarya Zone to the south (Figure 1a). It has a very thick (c. 9000 m) Cenozoic basinal infillings (Figure 1b) (Gürgey and Batı, 2018; Okay et al., 2023; Perinçek et al., 2015; Siyako, 2006; Turgut and Eseller, 2000). More importantly, the basin hosts most of the natural gas and limited oil resources of Türkiye (Huvaz et al., 2007); nevertheless, several mineable coal seams are also located in the basin within the Cenozoic basinal infillings. Early exploration studies during the 1970s show that there are eleven coal seams (upwards from I to XI), of which seven (I to VII) are economic, and located in the latest Early-Late Oligocene Danişmen Formation (Lebküchner, 1974). These seams are exploiting different coalfields in the southwestern and north-eastern parts of the Thrace Basin. Even though the sedimentological features, source rock potential, and depositional environment of certain Palaeogene formations in the basin are well-known due to the existence of hydrocarbon systems, limited studies were conducted on the coal seams within the latest Early-Late Oligocene Danişmen Formation (Çelik et al., 2017; Erarslan and Örgün, 2017; Erarslan et al., 2014, 2020; Karayiğit et al., 2022a; Tuncalı et al., 2002). These studies show that coal seams in the Danişmen Formation are commonly characterized by low ash yields, high total huminite contents, and relatively high total S, volatile matter, and B contents. Furthermore, these studies also indicate that the palaeomires in the Thrace Basin were mostly accumulated under forested mire conditions within flood plains, and some of these mires were also opened to marine influence (Çelik et al., 2017; İslamoğlu et al., 2010; Karayiğit et al., 2022a; Leibkühner, 1974; Siyako, 2006). Therefore, high total S and B contents could be related to marine influence. However, detailed coal mineralogy studies from the Malkara and Yeniköy coalfields also noted that the relatively high total S contents could also be controlled by anoxic marine conditions, while clastic influxes from the Strandja Massif might also cause elevations in the B contents of these seams. Also, coal

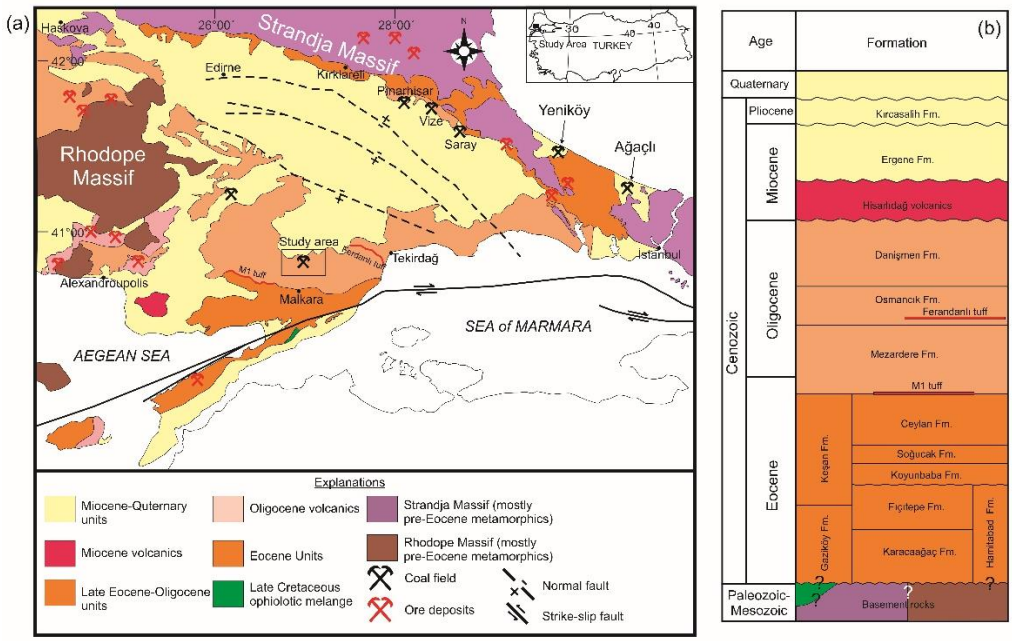

Figure 1: (a) Geological map of the Thrace Basin (modified from Karayiğit et al. (2022a), Siyako (2006), Okay et al. (2023), and (b) generalized stratigraphic column of the Thrace Basin (modified from Gürgey and Batı (2020), Karayiğit et al. (2022a), Siyako (2006) and Okay et al. (2023).

Şekil 1: *(a) Trakya Havzası'nın jeolojik haritası (Karayiğit vd. (2022a), Siyako (2006) ve Okay vd. (2023)'den değiştirilerek alınmıştır) ve (b) Trakya Havzası'nın genelleştirilmiş stratigrafik kolon kesiti (Gürgey ve Batı (2020), Karayiğit vd. (2022a), Siyako (2006) ve Okay vd. (2023)'den değiştirilerek alınmıştır).*

seams in the Malkara coalfield display different paleontological and sedimentological features (İslamoğlu et al., 2010; Karayiğit et al., 2022a; Lebküchner, 1974; Şafak, 2019). For instance, the precursor peat mires of coal seams in the northern and western parts of the coalfield (e.g., Şahin, Pirinçeşme, and Hasköy areas) were accumulated flood plain and freshwater conditions, while palaeomires of coal seams in the sectors in the eastern part (e.g., Pullukçu area) seem to be formed under back mangrove conditions, where open to influence of seawater penetration (İslamoğlu et al., 2010; Karayiğit et al., 2022a). Considering the locations of coal-bearing areas in the Malkara coalfield (Figure 2), possible marine influence into palaeomires of the Seam-VI in the İbrice area could be possible. Nevertheless, the Seam-VI has not been investigated in detail to date. In this study, we aimed to investigate the mineralogical, petrographic, and geochemical properties of the Seam-VI and evaluate elemental enrichments and palaeoenvironmental conditions during the peat accumulation. The specific goal of this study is to compare the mineralogical and petrographic properties of the Seam-VI with those of other seams in the northern and eastern parts of the Thrace basin.

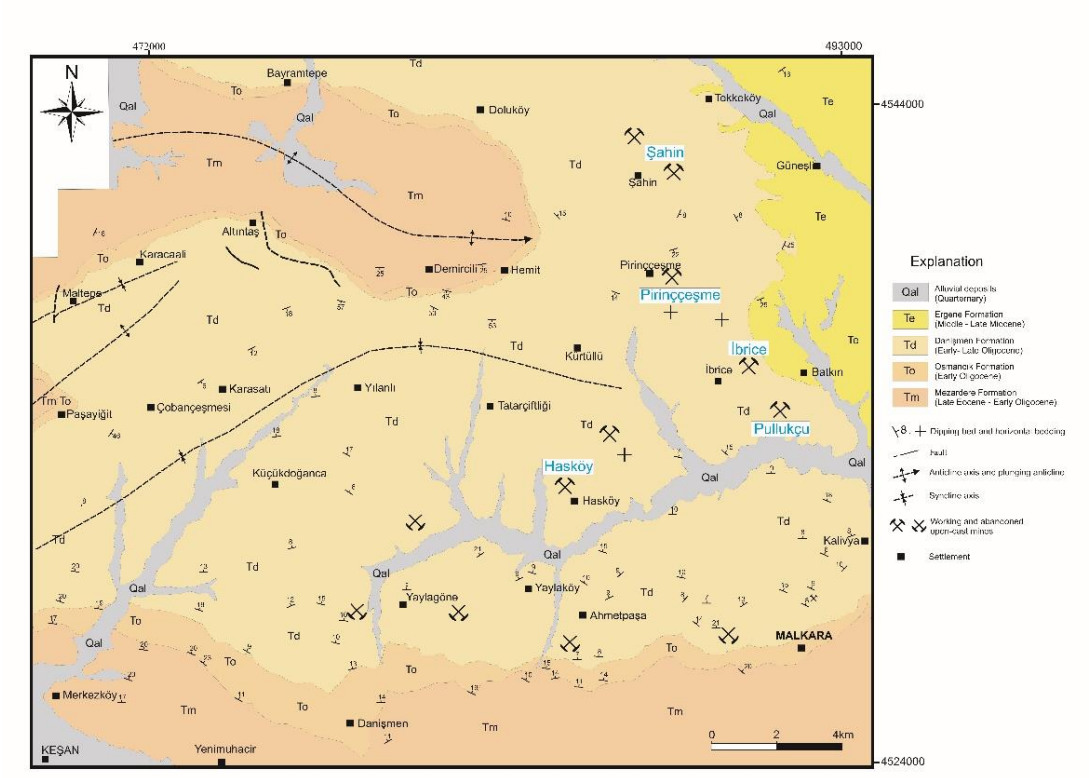

Figure 2: Geological map of the surrounding area of the İbrice area (modified from Karayiğit et al. (2022a).

Şekil 2: *İbrice sahası çevresinin jeolojik haritası (Karayiğit ve diğerleri (2022a)'dan değiştirilerek alınmıştır).*

GEOLOGY

The İbrice area (Malkara coalfield) is positioned in the southwestern part of the Thrace Basin (Figure 1a). Although pre-Cenozoic basement rocks do not crop out in the study area, the basement rocks mainly compose of metamorphic and magmatic rocks of the Strandja Massif in the northern parts of the Thrace Basin and the Rhodope Massif in the western parts of the basin, and ophiolitic rocks of Cretaceous-Paleogene Çetmi Mélange in the southern parts of the basin (Figure 1a-b). The Cenozoic basinal infillings, which crop out in the study area, are, from bottom to top, the Late Eocene-Early Oligocene Mezardere Formation, the Early Oligocene Osmancık Formation, the Early-Late Oligocene Danişmen Formation, and the Middle-Late Miocene Ergene Formation (Figure 2). The Mezardere Formation, locally also known as Mezardere shales, consists of an alternation of shale, marl, and sandstone, and tuffite layer were reported from the lower parts of the formation. Previous paleontological and sedimentological studies have reported that a major sea-level drop in the Eastern Paratethys developed during the Late Eocene and Early Oligocene; as a result, several transgressions and regressions also developed in the Thrace Basin during this

period (Gürgey and Batı, 2018; Turgut and Eseller, 2000). Hence, the Mezardere Formation was deposited under prodelta and shallow marine conditions. The Osmancık Formation gradually overlies the Mezardere Formation and composes mainly of sandstone and shale, and, to a lesser extent, pebblestones and limestones. Furthermore, uneconomic coal seams and tuffite layers were also reported from this formation. The previous studies indicate that the Osmancık Formation mainly deposited under front delta and shallow marine conditions (Siyako, 2006; Turgut and Eseller, 2000).

MATERIAL AND METHODS

A total of fifteen samples (eight coal, and seven roof and intercalation samples) were gathered from the Seam-VI in the İbrice area using the channel sampling method (Figure 3). The lithotype descriptions of coal samples were done following the International Committee for Coal and Organic Petrography (ICCP) nomenclature on site (ICCP, 1993). Standard proximate, ultimate, and calorific analyses were conducted following the American Society for Testing and Materials (ASTM) standards using LECO TGA-601, SC-144DR, TruSpec, and AC 350 equipment at Hacettepe University (ASTM D3174, 2020; ASTM D3175, 2020; ASTM D3302/D3302M, 2022; ASTM D5373, 2021; ASTM D5865/D5865M, 2019). Coal petrography studies were conducted on polished blocks using a Leica DM4000M microscope, and ICCP classification was followed for maceral descriptions (ICCP, 2001; Pickel et al., 2017; Sýkorova et al., 2005). The random huminite reflectance measurements (%Rr) were done from ulminite B according to the International Organization for Standardization (ISO) 7404–5 (2009) standard. Rigaku D/MAX 2200 PC equipment equipped with CuKα radiation was used for X-ray powder diffraction (XRD) analyses, and Rietveld-based TOPAS-3 software is used for semi-quantitative mineralogical composition determination. The XRD-clay fraction (XRD-CF) analyses were conducted from selected five samples (18-13/01, 18-13/06, 18-13/11 and 18-13/14) according to methodology described in Karayiğit et al. (2022c). Major oxide contents, and minor and trace element compositions of studied coal and organic mudstone samples were conducted from ashed samples at 450˚C using a muffle furnace, according to Nadkarni (1980) at Hacettepe University. Major oxide contents

were determined from pellets using XRF equipment according to the ASTM D-4326 standard at Standart Laboratories S.A, Kocaeli-Türkiye. The ashed samples were sequentially digested using HF, HCL, and nitric acid, and the diluted samples were analyzed using inductively coupled plasma-optical emission spectrometry (ICP-OES) according to the ISO-11885 standard at Standart Laboratories S.A. The accuracy of analyses was crosschecked using international and internal standards. Selected polished blocks of three coal samples (18-13/03, 18-13/04, and 18-13/10) were coated with carbon and examined under a Thermo Fisher Scientific FEI Quanta 400 MK2 SEM-EDX microscope at the General Directorate of Mineral Research and Exploration (MTA) to identify possible accessory mineral phases and to have a better understanding of the elemental compositions.

RESULTS

Standard coal quality

The coal samples from the Seam-VI exhibit a black colour on-site and contain bands of xylite and/or clayey material, and fossil shell remains. The xylite-rich and mineral-rich lithotypes were identified from the studied coal samples (Figure 3). Although it is not officially described by the

ICCP (1993), xylite-rich lithotype could be divided into xylo-detritic and detro-xylitic according to the presence of clastic bands within xylite-rich coals (Fabiańska and Kurkiewicz, 2013; Kolcon and Sachsenhofer, 1999; Karayiğit et al., 2021). In the studied Seam-VI, the xylo-detritic sub-lithotype, which is clayey bands-bearing xylite-rich coal, is also identified from one sample (18–13/09).

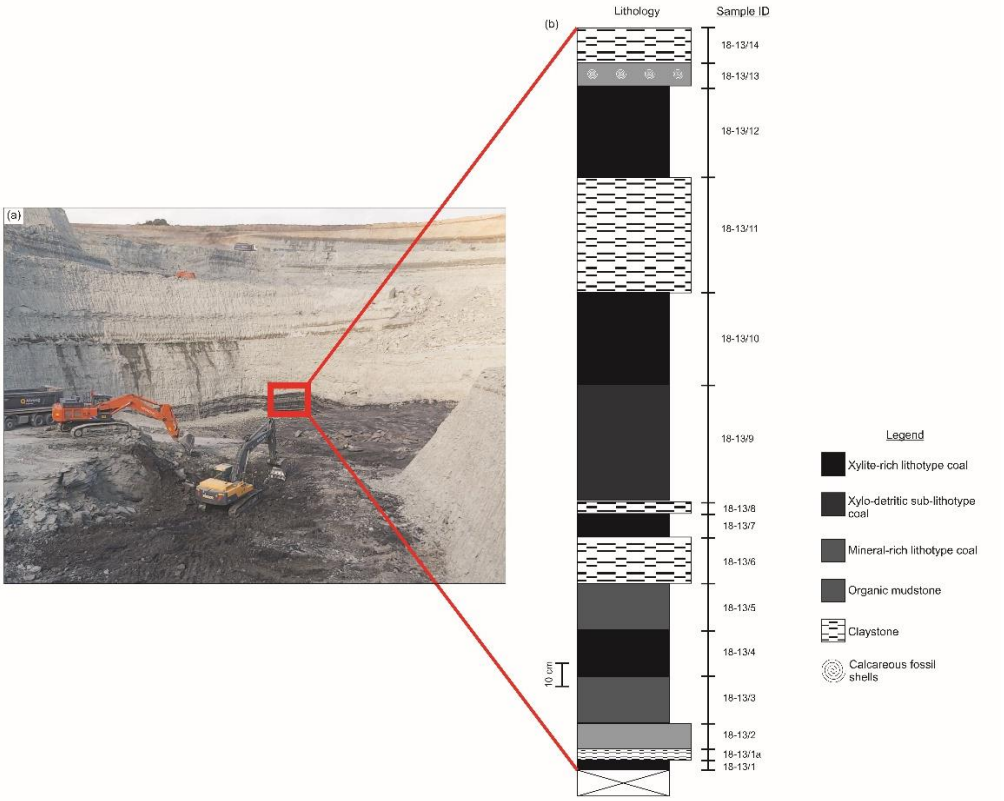

Figure 3: General view of (a) an open-cast mine and (b) the sampling profile studied in the İbrice area.

Şekil 3: *(a) İbrice sahasındaki açık ocağın genel görünümü ve (b) çalışma kapsamında çalışan kesit.*

Considering the presence of xylite-rich and mineral-rich lithotypes in the Seam-VI, the coal samples display on a dry basis variable ash yields, volatile matter, total C and H contents, and gross calorific values (Table 1 and Figure 4). As expected, xylite-rich lithotype-bearing samples generally display low ash yields, and high total C contents and gross calorific values, while mineral-rich ones show significantly high ash yields and low total C and gross calorific values (Table 1 and Figure 4). As can be seen in the coal petrography section, the distribution of H contents seems to be related to maceral compositions. The total S contents of coal samples are generally lower than 2% on a dry basis; nevertheless, samples in which pyrite is an abundant phase, have relatively higher total S (up to 4.1% on a dry basis) contents than the

other coal samples (Table 1). Furthermore, carbonaceous shale (18-13/02) and organic mudstone (18-13/13) samples have ash yields higher than 50.0% on a dry basis (Table 1 and Figure 4). The samples from the İbrice area have similar ash yields, total C, H and total S contents, and gross calorific values, to those from other coal mining areas in the Malkara coalfield.

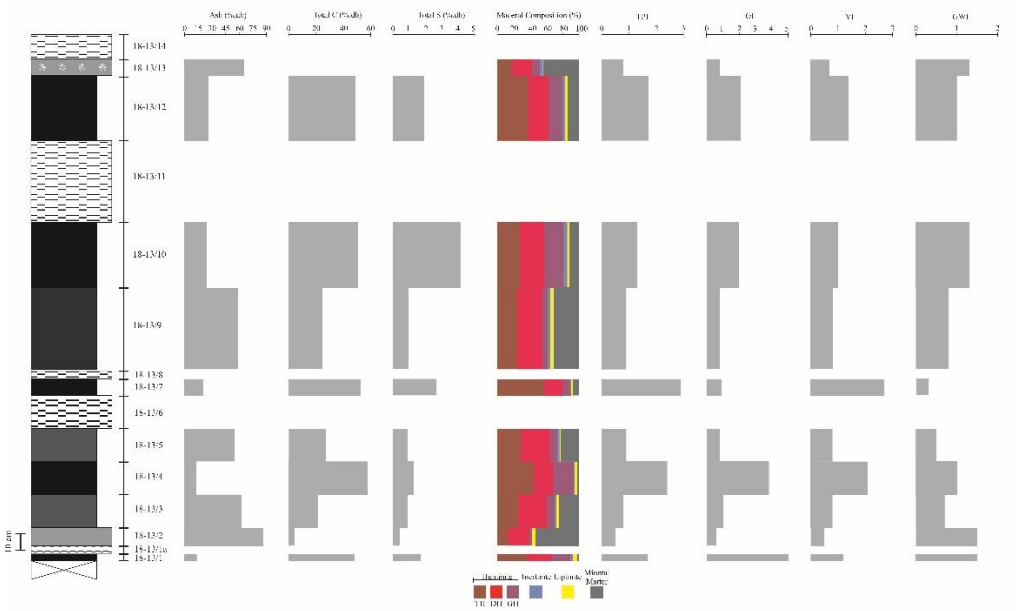

Figure 4: Vertical distrubition of ash, total C and S, macearal compositions and coal facies indicies through sampling profile (for legend of lithostratigraphic column, see Figure 3).

Şekil 4: *İncelenen örneklere ait kül, toplam C ve S, maseral içerikleri ve kömür fasiyes parametrelerinin örnekleme profil boyunca düşey dağılımı (litostratigrafik sütun kesitin açıklaması için Şekil 3'bakınız).*

Coal Petrography

Huminite is the predominant maceral group in the coal samples, while liptinite and inertinite group macerals display variable proportions (Table 2 and Figures 5 and 6). Telohuminite subgroup macerals are commonly identified in the samples (Figure 5). Ulminite is the most common telohuminite subgroup maceral in the samples (Figure 5a-b), whereas textinite has relatively higher proportions in xylite-rich lithotype samples (Figure 5a-b). Atrinite is a more common detrohuminite subgroup maceral in the mineral-rich lithotype coal, shale, and organic mudstone samples, and it is mostly observed within the clay mineral matrix (Figure 5c). Densinite displays relatively higher proportions in the xylite-rich lithotype coal samples, and sporinite and inertodetrinite are generally associated with densinite (Figure 5d). Corpohuminite is the predominant gelohuminite subgroup maceral in the coal samples and has significantly higher proportions in xylite-rich litotype coal samples (Table 2). Corpohuminite is mostly identified as corpohuminite accumulation and cell-lumen infillings of textinite (Figure 5a, b and e).

Levigelinite is another common gelohuminite subgroup maceral, while porigelinite is rarely identified within the cell-lumens of textinite (Figure 5f).

Liptodetrinite and sporinite, which are associated with detrohuminite macerals, are the common liptinite group macerals, while cutinite, resinite, and alginite are rarely observed (Table 2 and Figure 6a-b). Inertinite displays low proportions in the samples (<3.0% on the whole coal-basis), and inertodetrinite and funginite, with variable morphologies, are

Table 1: The results of proximate, ultimate and calorific analyses of studied coal and shale samples (GCV: gross calorific value; as-rec.: as received basis; db: on dry basis; XC: xylite-rich lithotype; XCD: xylo-detritic sub-lithotype; MRC: mineral-rich lithotype; CS: carbonaceous shale, OM: organic mudstone, na: not available, *oxygen content is calculated by subtraction [O = 100 − (C + H + S + N + ash)] on dry basis)).

Çizilge 1: *İncelenen kömür ve şeyl örneklerine ait kaba kimyasal ve elementer ile kalorifik analizlere ait sonuçlar (GCV: üst ısıl değer; as-rec.: orijinal baz; db: kuru baz; XC: ksilitçe zengin litotip; XCD: ksilo-detritik altlitotip; MRC: mineralce zengin litotip; CS: karbonlu şeyl, OM: organik çamurtaşı, na: veri yok, * oksijen içeriği kuru bazda O = 100 − (C + H + S + N + kül) formülüne göre hesaplanmıştır).*

Sample	Lithotype/ Lithology	Moisture wt%, as-rec	Ash wt%, db	VM	GCV kcal/kg, db	C	H	N	S	O*
						wt%, db				
18-13/13	OM	20.8	65.5	28.5	1472	na	2.4	0.4	na	na
18-13/12	XC	29.7	26.7	39.6	4800	48.9	4.2	1.4	1.9	17.0
18-13/10	XC	21.4	24.7	41.9	4913	50.8	4.2	1.4	4.1	14.8
18-13/09	XCD	20.5	58.8	25.5	2480	24.6	3.3	0.8	0.9	11.6
18-13/07	XC	27.5	21.1	40.0	5192	52.5	4.4	1.1	2.7	18.2
18-13/05	MRC	22.5	55.4	26.2	2667	27.2	3.2	0.8	0.9	12.4
18-13/04	XC	30.2	13.2	43.0	5637	57.8	4.5	1.8	1.3	21.4
18-13/03	MRC	20.7	63.0	24.3	3752	21.2	3.0	0.7	0.9	11.2
18-13/02	CS	18.6	86.7	12.2	na	4.5	2.2	0.2	0.4	6.0
18-13/01	XC	32.2	13.7	42.9	5663	57.6	4.6	1.9	1.7	20.5

the main inertinite group macerals (Figures 5d and 6c). Furthermore, funginites are identified during SEM studies (Figure 7). Since the Danişmen Formation is known for its rich fungal flora (Çelik et al., 2017; Ediger, 1981; Ediger and Alişan, 1989; Elsik et al., 1990), the diverse morphologies of funginite are expected. Similar observations have been reported in other coal seams within the Malkara coalfield (Karayiğit et al., 2022a), where fusinite and semifusinite are barely identified. Mineral matter contents vary (2.2–53.8% on a whole-coal basis), and

mineral matter identified under incident white light include clays, framboidal pyrite grains (individual or aggregates), cleat/fracture pyrite infillings, syngenetic carbonate bands, siderite nodules, and quartz grains (Figures 5c and 6 d-f). Furthermore, calcareous fossil shell remains are also observed. In comparison with other coal mining areas in the Malkara coalfield (Karayiğit et al., 2022a), the studied samples display similar maceral compositions. As can be seen in the mineralogy section, syngenetic carbonate bands and siderite nodules are less common, and replacement carbonates were not observed in the Seam-VI.

The mean %Rr values of analysed samples are ranging between 0.40±0.02% and 0.41±0.01% (Table 2). These values are close to reported mean %Rr values from other coal mining areas in the Malkara coalfield (Karayiğit et al., 2022a), and slightly higher than the %Rr values of other coalfields (e.g., Pınarhisar and Yeniköy) close to Standrja massif (Çelik et al., 2017; Erarslan and Örgün, 2017).

Table 2: Maceral composition of studied coal and shale samples (vol.%, on whole basis), mean random huminite reflectance (%Rr) values of coal samples (Stdv: standard deviation).

Çizelge 2: *İncelenen kömür ve şeyl örneklerine ait maseral içerikleri (tüm bazda, hacimsel %) ve kömür örneklerine ait ortalama hüminit yansıtma (%Rr) değerleri (Stdv: standart sapma).*

Maceral	Sample									
	18-13/1	18-13/2	18-13/3	18-13/4	18-13/5	18-13/7	18-13/9	18-13/10	18-13/12	18-13/13
Textinite	11.6	0.5	2.8	16.7	8.2	27.4	5.1	10.5	13.1	2.4
Ulminite	25.1	12.3	22.2	28.4	20.3	30.5	19.0	17.1	23.8	15.2
Telohüminite	*36.8*	*12.8*	*25.0*	*45.2*	*28.5*	*57.9*	*24.1*	*27.6*	*36.9*	*17.6*
Attrinite	0.6	25.8	31.9	2.0	31.1	18.7	27.0	12.4	10.6	24.7
Densinite	29.9	0.3	3.1	20.6	5.2	3.0	4.0	17.3	15.6	0.7
Detrohüminite	*30.5*	*26.1*	*35.0*	*22.7*	*36.3*	*21.6*	*31.0*	*29.7*	*26.1*	*25.5*
Levigelinite	1.8	1.3	3.6	5.0	2.2	0.5	1.6	4.4	2.8	3.0
Porigelinite	0.4				0.2	0.9	0.1	0.3		0.3
Corpohuminite	20.0	1.7	6.2	20.8	6.1	8.0	4.6	17.9	14.2	5.6
Gelohüminite	*22.2*	*3.0*	*9.8*	*25.8*	*8.5*	*9.4*	*6.3*	*22.7*	*17.0*	*8.9*
Huminite	***89.5***	***41.9***	***69.8***	***93.7***	***73.3***	***89.0***	***61.4***	***80.0***	***79.9***	***52.0***
Fusinite	0.4		0.4		0.7		0.2	0.3	0.3	0.3
Inertodetrinite	1.3	0.4	0.3	0.0	0.3	0.0	0.5	1.1	0.8	0.7
Funginite	1.5	0.2	1.4	1.1	1.6	0.9	2.6	2.7	1.7	1.6
Semifüsinite						0.2	0.4	1.1		0.3
Inertinite	***3.1***	***0.6***	***2.1***	***1.1***	***2.7***	***1.0***	***3.7***	***5.2***	***2.8***	***2.9***
Sporinite	2.6	1.5	1.9	1.5	0.6	0.9	1.4	1.3	1.9	0.2
Cutinite	0.4	0.3		0.9	0.0	0.0		0.3		
Resinite	0.4	0.1		0.4	0.1	0.7	0.4	0.6	0.6	
Alginite	0.4	0.3			0.1				0.2	0.1
Liptodetrinite	1.3	1.5	1.0	0.2	0.7	0.9	1.6	0.6	1.1	0.4
Liptinite	***5.0***	***3.7***	***2.9***	***3.0***	***1.6***	***2.4***	***3.3***	***2.9***	***3.7***	***0.7***
Mineral Matter	***2.4***	***53.8***	***25.2***	***2.2***	***22.4***	***7.5***	***31.5***	***11.6***	***13.5***	***44.3***
Mean %Rr				0.41				0.40	0.40	
Stdv (±)				0.01				0.01	0.02	

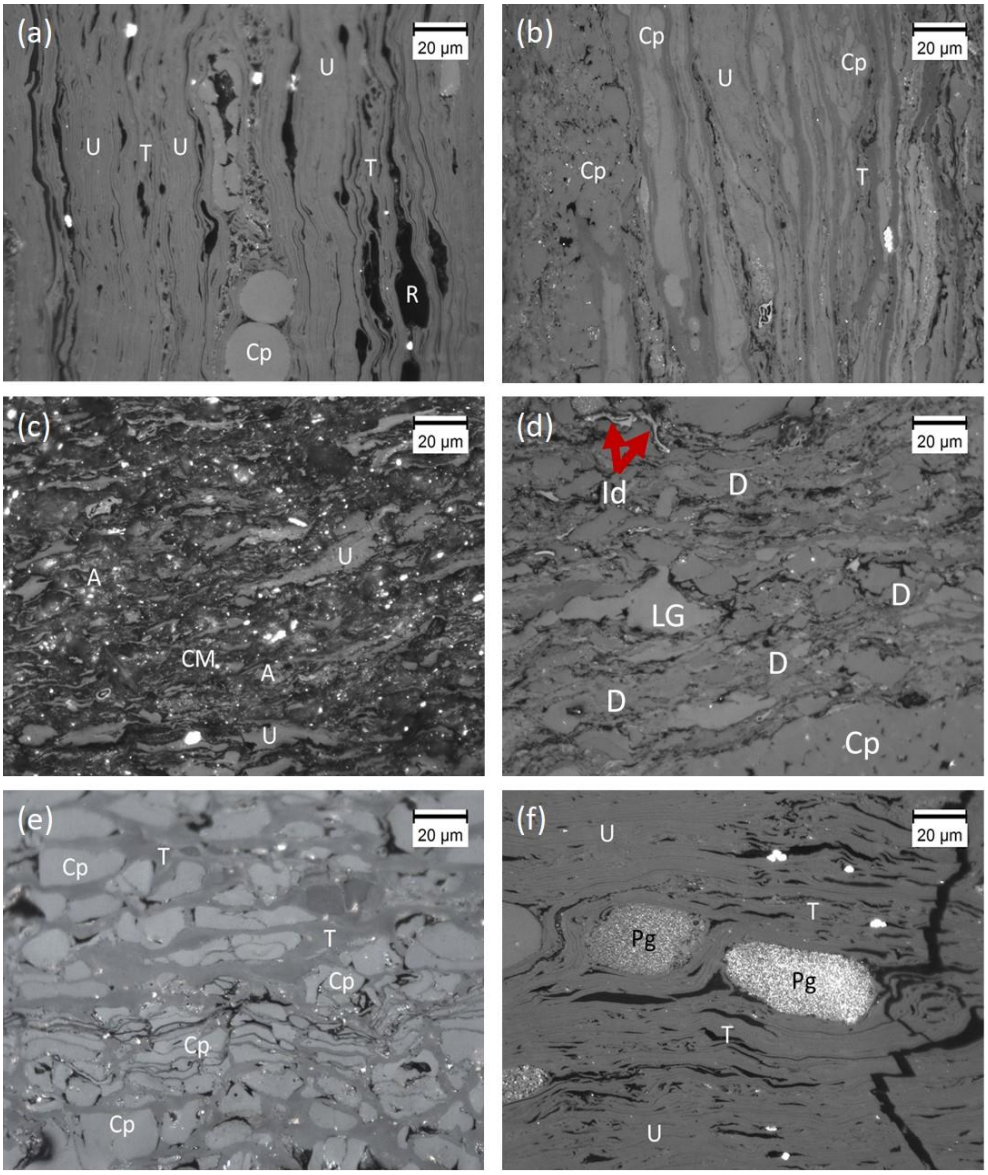

Figure 5: Photomicrographs of coal and shale samples from the Seam-VI. All photomicrographs are taken under incident white light (a-f), oil immersion, 500 × total magnification. A: attrinite, CM: clay minerals, Cp: corpohuminite, D: densinite, Id: inertodetrinite, Pg: porigelinite, R: resinite, LG: levigelinite, T: textinite, U: ulminite.

Şekil 5: *Damar-VI'dan alınan kömür ve şeyl örneklerinin fotomikrografları. Bütün mikrofotograflar üstten aydınlatmalı normal ışık kullanılarak (a-f), 500× toplam büyütmeli yağlı objektifte çekilmiştir. A: atrinit, CM: kil mineralleri, Cp: korpohüminit, D: densinit, Id: inertodetrinit, Pg: porigelinit, R: resinit, LG: levigelinit, T: tekstinit, U: ülminit.*

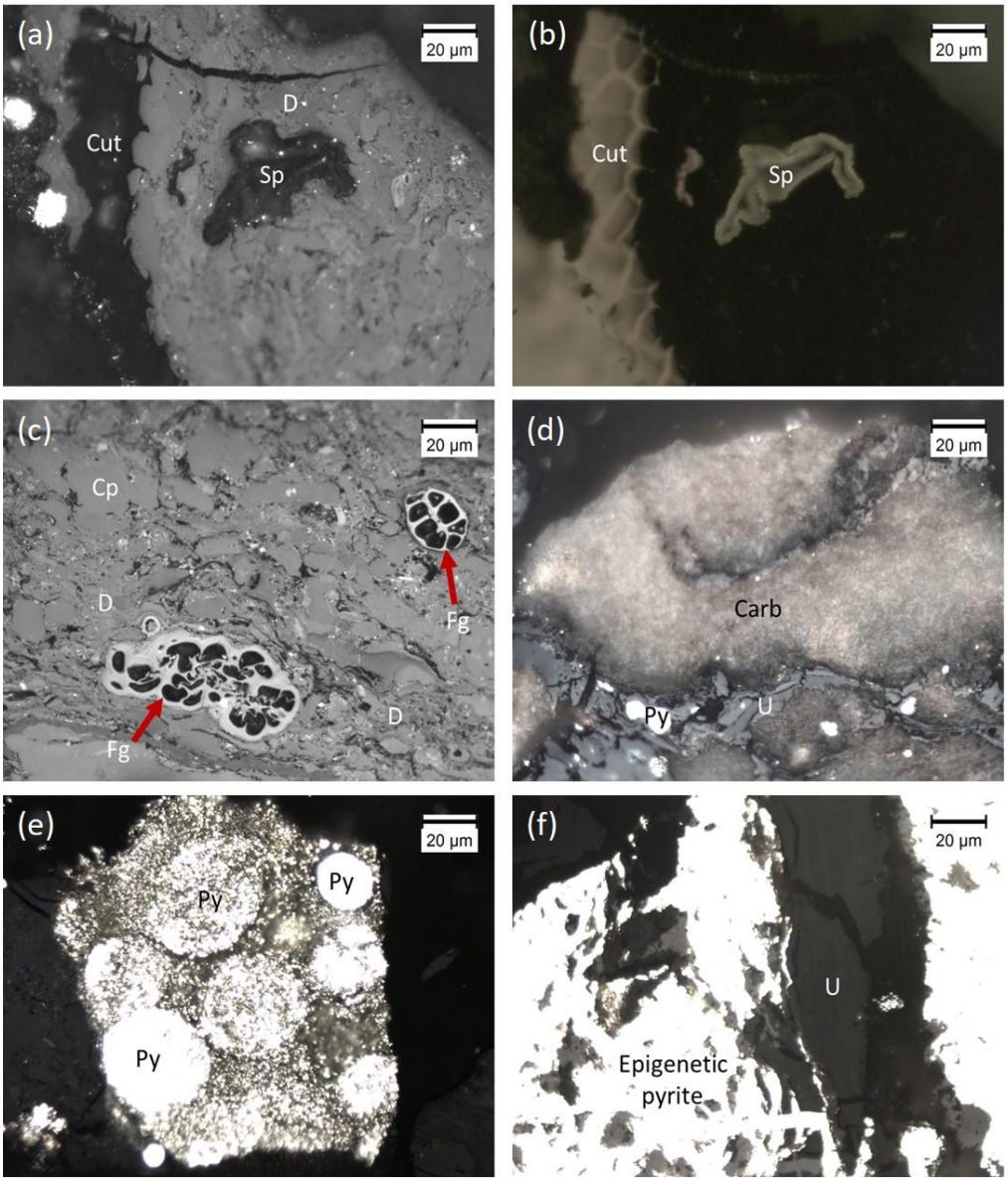

Figure 6: Photomicrographs of coal and shale samples from the Seam-VI. All photomicrographs are taken under incident white light (a,d-f) and blue-light excitation (b), oil immersion, 500 × total magnification. Carb: carbonate mineral, Cp: corpohuminite, Cut: cutinite, D: densinite, Fg: funginite, Py: pyrite, Sp: sporinite, U: ulminite.

Şekil 6: *Damar-VI'dan alınan kömür ve şeyl örneklerinin fotomikrografları. Bütün mikrofotograflar üstten aydınlatmalı normal ışık (a, c-f) ve UV mavi ışık (b) kullanılarak, 500× toplam büyütmeli yağlı objektifte çekilmiştir. Carb: karbonat minerali, Cp: korpohuminit, Cut: kütinit, D: densinit, Fg: funginit, Py: pirit, Sp: sporinit, U: ülminit.*

Table 3: Semi-quantitative mineralogical composition of the studied coal and non-coal samples based on XRD and SEM-EDX analyses (+++ = dominant phase (> 30%), ++ = abundant phase (5-30%), + = minor phase (< 5%) by XRD, a: accessory mineral detected by SEM-EDX) (Abbreviations: XC: xylite-rich lithotype; XCD: xylo-detritic sub-lithotype; MRC: mineral-rich lithotype; CS: carbonaceous shale, OM: organic mudstone, Ap: apatite, Brt: barite, Dol: dolomite, Feld: feldspars, Pnt: pentlandite, Sph: sphalerite and Zrn: zircon).

Çizelge 3*: XRD ve SEM-EDX analizlerine göre incelenen kömür ve kömür dışı örneklere ait yarı kantitatif mineralojik bileşimleri (XRD analizlerine göre +++ = baskın faz (> 30%), ++ = bol faz (5-30%), + = minör faz (< 5%), a: SEM-EDX tarafından tespit edilen aksesuar faz) (Kısaltmalar; XC: ksilitçe zengin litotip; XCD: ksilo-detritik altlitotip; MRC: mineralce zengin litotip; CS: karbonlu şeyl, OM: organik çamurtaşı; Ap: apatit, Brt: barit, Dol: dolomit, Feld: feldspatlar, Pnt: pentlandit, Sph: sfalerit ve Zrn: zirkon).*

Sample	Lithotype/ Lithology	Quartz	Clay minerals	Feld	Biotite	Zrn	Calcite	Dol	Aragonite	Siderite	Pyrite	Sph	Pnt	Brt	Ap	Ti-oxide
18-13/14	Claystone	++	+++	+			++	+		+	+					
18-13/13	OM	++	+++	++			++		++		+					
18-13/12	XC	++	+++	++							+					
18-13/11	Claystone	++	+++	+			+	+			+					
18-13/10	XC	++	+++	a			a	a	++		++	a			a	
18-13/09	XCD	+++	+++	++			+									
18-13/08	Claystone	++	+++				++	+		+						
18-13/07	XC	++	+++								++					
18-13/06	Claystone	++	+++	+			++	++								
18-13/05	MRC	++	+++	+++												
18-13/04	XC	+++	+++	a	a	a		a		a	+			a	a	
18-13/03	MRC	++	+++	++	a		a				+		a	a	a	a
18-13/02	CS	++	+++	++												
18-13/01	XC	+++	+++								+					
18-13/01a	Claystone	++	+++	+				++			+					

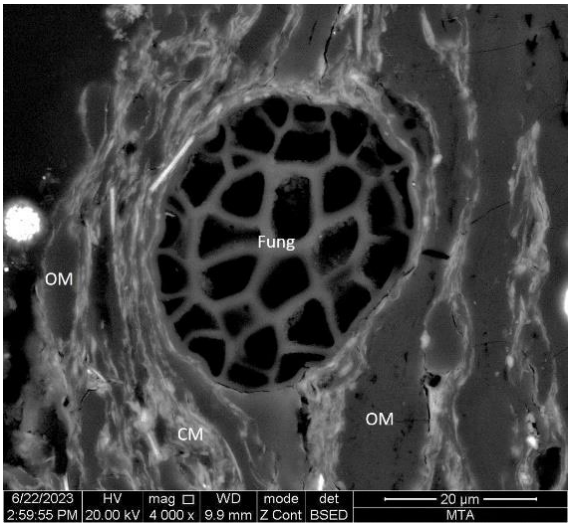

Figure 7: SEM backscattered image of funginite. CM: clay mineral, Fung: funginite, OM: organic matter.

***Şekil 7**: Funginit maseraline ait SEM geri saçılım görüntüsü. CM: kil minerali, Fg: fungini, OM: organik madde.*

Mineralogy

The minerals identified using XRD-whole rock analysis are clay minerals, quartz, pyrite, calcite, dolomite, and feldspars (Table 3). Siderite is identified from one coal sample (18-13/08) and rock sample (18-13/14), whereas it is identified as an accessory phase from one coal sample (18-13/04). Aragonite is detected in two samples (18-13/10 and /13), both of which contain fossil shell remains (Table 5). The SEM observations agree with XRD data, and apatite, barite, biotite, pentlandite, sphalerite, Ti-oxide, and zircon are also determined as accessory phases in the coal samples (Table 3).

Clay minerals are the dominant phases in all studied samples (Table 3), and the identified clay minerals are smectite, illite, chlorite, and kaolinite according to XRD-CF data. Quartz is mostly an abundant phase, and in a few samples, it is the dominant phase. Feldspars are present as minor to abundant phases in mineral-rich lithotype coals and some intercalation samples (Table 3). Calcite and dolomite are present as minor to abundant phases in inorganic samples, while calcite is detected as a minor to accessory phase in coal samples (Table 3). As mentioned above, aragonite is detected as an abundant phase in fossil shell remains-bearing samples. Pyrite is mostly a minor phase in the samples, and it is commonly abundant phase in xylite-rich lithotype coal samples (Table 3).

Geochemistry

The major oxide contents of the analysed ashed samples vary (Table 4), and the SiO_2, Al_2O3 and K_2O contents of mineral-rich lithotype coal samples, carbonaceous shale,

and organic mudstone samples are generally higher than those of xylite-rich lithotype coal samples. In contrast, xylite-rich lithotype coal samples display relatively higher CaO and Fe_2O_3 contents (Table 4). These differences could be related to the existence of clay mineral bands in the mineral-rich lithotype coal samples, carbonaceous shale, and organic mudstone samples, as well as possibly organically bound Ca in xylite-rich samples. Additionally, there are not any significant differences in Na_2O, MgO, and TiO_2 contents among the samples. These factors could also explain the lack of well-defined vertical variations in major oxide contents throughout the sampling profile (Figure 8a).

The average concentrations on a whole-coal basis of B, P, Mn, Sr, and Ba in coal and carbonaceous shale (e.g.18-13/02) samples are higher than 100 ppm, while the average concentrations of Li, V, Cr, Ni, Cu, Zn, Ge, and Mo in are between 10 to 100 ppm (Tables 4 and 5). The remaining elements in the coal samples display average concentrations on a whole-coal basis lower than 10 ppm (Tables 4 and 5). In order to determine elemental enrichments in the studied profile, concentration coefficient (CC) were calculated according to Dai et al. (2015). These calculations are based on dividing the average concentrations of coal and shale samples by Clarke values for low-rank coals and sedimentary rocks reported in Ketris and Yudovich (2009). The calculated CC values for coal samples indicate significant enrichments for Mn (CC=14.9) and Ni (CC=10.8), while Ge (CC=7.2) and Mo (CC=5.4) are classified as enriched (Table 5). The slightly enriched elements in the coal samples are B (CC=2.3), Cr (CC=2.8), Co (CC=2.1), and Sr (CC=3.0). The CC values for Li, P, Sc, V, Cu, Zn, As, Y, Cd, Ba, and Pb are close to low-rank coal averages ($0.5<CC<2.0$), whereas the remaining elements are depleted ($CC<0.5$).

DISCUSSIONS

Coal Rank

The rank determination of coals is mostly based on mean %Rr values; nevertheless, the sole usage of this parameter, particularly for Cenozoic coals, does not provide a proper rank estimation (O'Keefe et al., 2013). In some cases, the %Rr values of ulminite B macerals in xylite-rich coals could be suppressed due to the existence of H-rich compounds in peat-forming plants (Çelik et al., 2017; Papanicolaou et al., 2000; Sykes et al., 1994). Like the other coal seams within the Malkara coalfield (Karayiğit et al., 2022a), H contents display a moderately positive correlation with total telohuminite contents. Therefore, the mean %Rr values of the coal samples from the İbrice area should be combined with ash yields and gross calorific values in order to have better rank estimations. The mean %Rr values, along with ash yields and gross calorific values of the studied samples, show that xylite-rich lithotype coal samples are medium to high-grade low-rank A based on the ECE-UN (1988) classification and low- to medium-ash low-rank A based on the ISO 11760 (2005) classification. As expected, mineral-rich lithotype coal samples are low- to medium-grade low-rank B and medium- to high-ash low-rank A according to the ECE-UN (1988) and ISO 11760 (2005) classifications, respectively.

As mentioned previously, the studied samples have relatively lower mean %Rr values than working coal seams in the Hasköy, Şahin, and Pirinççeşme areas in the Malkara coalfield. Although the difference is not high, these differences could be related to the relatively deeper recent burial depths of the working coal seams in the Hasköy, Şahin, and Pirinççeşme

Table 4: Elemental composition of the studied coal (on whole coal basis) and shale samples (on whole rock-basis). All results in ppm, expect otherwise cited (Abbreviations: XC: xylite-rich lithotype; XCD: xylo-detritic sub-lithotype; MRC: mineral-rich lithotype; CS: carbonaceous shale, OM: organic mudstone, na: not available).

Çizelge 4: *İncelenen kömür (tüm kömür bazında) ve şeyl örnekerlerinin (tüm kayaç bazında) elementel içerikleri. Bütün sonuçlar ppm olarak sunulmuştur, aksi taktirde belirtilmiştir (Kısaltmalar: XC: ksilitçe zengin litotip; XCD: ksilo-detritik altlitotip; MRC: mineralce zengin litotip; CS: karbonlu şeyl, OM: organik çamurtaşı, na: veri mevcut değil).*

Element	18-13/1	18-13/2	18-13/3	18-13/4	18-13/5	18-13/7	18-13/9	18-13/10	18-13/12	18-13/13
Lithotype/ Lithology	XC	CS	MRC	XC	MRC	XC	XCD	XC	XCD	OM
SiO_2 (%)	28.9	61.9	56.5	30.5	55.9	38.3	58.1	31.5	47.5	48.7
TiO_2 (%)	0.68	0.68	0.78	0.59	0.80	0.63	0.74	0.57	0.92	0.59
Al_2O_3 (%)	14.0	19.6	19.0	12.6	19.6	15.8	18.7	14.2	17.7	15.4
Fe_2O_3 (%)	11.0	7.4	8.4	11.0	8.6	17.9	8.3	18.0	9.0	6.4
MgO (%)	6.5	4.8	5.2	7.5	5.3	4.5	5.0	4.2	4.6	4.1
CaO (%)	13.9	0.7	3.2	15.2	2.2	7.1	1.9	12.6	6.6	18.5
Na_2O (%)	1.5	1.0	1.1	1.7	1.2	1.0	1.0	0.9	1.1	0.9
K_2O (%)	0.5	2.7	2.9	1.5	2.8	1.6	2.8	1.3	2.1	1.8
Li	2.6	7.9	13.1	2.1	14	6.6	21	6.1	19	8.3
Be	1.7	0.24	0.47	0.61	0.47	0.41	0.49	0.78	0.77	0.58
B	137	38	72	153	93	197	66	143	141	50
P	78	254	392	195	514	191	210	375	213	354
Sc	1.4	3.9	6.5	2.6	5.8	3.5	4.4	3.3	4.4	4.0
V	8.6	44	50	14	42	26	30	18	49	33
Cr	7.1	50	81	16	63	27	71	24	24	56
Mn	31	115	13701	42	118	49	213	68	53	345
Co	2.1	11	17	3.1	19	8.6	9.1	5.7	7.2	8.9
Ni	30	157	199	18	184	75	106	72	54	100
Cu	6.6	26	25	6.6	22	7.3	19	8.3	15	19
Zn	8.0	75	76	11	60	19	55	18	32	45
Ge	5.3	17	19	5.4	17	13	15	17	8.6	14
As	3.7	3.7	9.1	2.1	2.3	4.1	1.1	11	4.6	13
Sr	338	217	344	370	342	306	323	498	403	616
Y	8.2	5.9	8.9	6.6	11.2	7.1	6.3	11.1	9.8	9.1
Zr	9.4	4.2	10	3.9	41	7.5	5.8	4.8	20	7.7
Nb	0.5	3.1	4.2	1.2	7.5	2.3	1.5	0.9	5.0	2.3
Mo	7.4	15	14	5.8	13.1	7.5	22	8.9	21	7.4
Cd	0.16	0.33	0.36	0.13	0.94	0.23	0.32	0.29	na	0.26
Ba	172	107	178	198	178	171	169	256	218	174
Pb	1.9	14	17	2.4	10	4.8	10	3.4	5.9	10

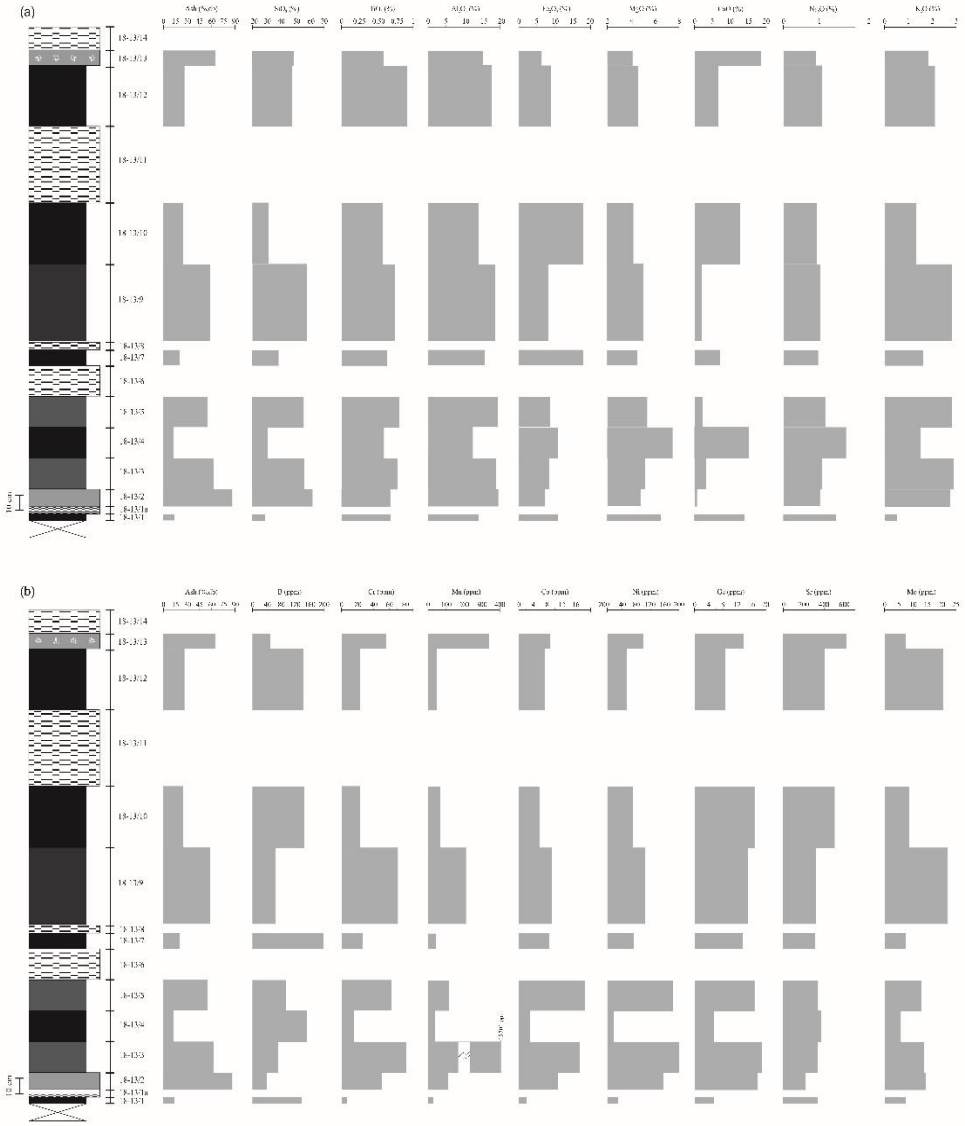

Figure 8: Vertical distrubition of (a) ash yield, SiO_2, TiO_2, Al_2O_3, CaO, Fe_2O_3, K_2O, MgO, and Na_2O; (b) B, Cr, Mn, Co, Ni, Ge, Sr and Mo (for legend of lithostratigraphic column, see Figure 3).

Şekil 8: *(a) kül, SiO_2, TiO_2, Al_2O_3, CaO, Fe_2O_3, K_2O, MgO ve Na_2O ile (b) B, Cr, Mn, Co, Ni, Ge, Sr and Mo elementlerin örnekleme profili boyunca düşey dağılımı (litostratigrafik sütun kesitin açıklaması için Şekil 3'bakınız).*

Table 5: Weighted average of the minor and trace elements (in ppm) for the coal samples from the Seam-VI in the İbrice area, and their comparison with Clarke values for low-rank coals (a: from Ketris and Yudovich (2009)). Elements in bold are enriched.

Çizelge 5: *İbrice sahasındaki Damar-VI'ya ait kömür örneklerinin ağırlıklı ortalamaları ve ortalamaların düşük kömürleşme derecesine sahip kömürlere ait Clarke değerleriyle karşılaştırılmaları (a: Ketris and Yudovich (2009)'dan alınmıştır). Koyu renkle belirtilen element değerleri zenginleşme sunmaktadır.*

Element	Clarke values for low-rank coals[a]	İbrice coal samples	Concentration coefficent (CC)
Li	10	10	1.0
Be	1.2	0.55	0.5
B	56	126	**2.3**
P	200	272	1.4
Sc	4.1	4.0	1.0
Ti	720	338	0.5
V	22	28	1.3
Cr	15	42	**2.8**
Mn	100	1493	**14.9**
Co	4.2	8.9	**2.1**
Ni	9	97	**10.8**
Cu	15	14	0.9
Zn	18	36	2.0
Ge	2	14	**7.2**
As	7.6	5.1	0.7
Sr	120	357	**3.0**
Y	8.6	8.0	0.9
Zr	35	8.1	0.2
Nb	11	2.2	0.2
Mo	2.2	12	**5.4**
Cd	0.24	0.31	1.3
Ba	150	188	1.3

areas than the İbrice area. Nevertheless, like other seams in the Malkara coalfield, Seam-VI displays higher mean %Rr values than working coal seams in the northern parts of the Thrace Basin (e.g., Yeniköy and Pınarhisar coalfields). According to thermal 1-D modelling, based on the mean %Rr values of Eocene and Oligocene formations in the oil and gas production fields in the Thrace Basin, major vertical tectonic movement from the Miocene to the Pliocene caused deeper burial depths in the central and southern parts of the basin (Huvaz et al., 2007). Furthermore, the thermal gradient around the central and southern parts of the basin was higher than the northern parts. Hence, as reported earlier by Karayiğit et al. (2022a), the differences in mean %Rr values of working coal seams between the study area and the northern parts of the Thrace Basin are expected.

Origin of Minerals

To determine the mode of occurrence of minerals in coal could provide data about water chemistry, redox, salinity, and hydrogeological conditions during the precursor peat

accumulation, as well chemistry of circulating fluids during coalification (Dai et al., 2020a; Ward, 2002, 2016). The XRD and SEM-EDX data of the coal and carbonaceous shale samples could imply that the identified minerals are mainly detritic and authigenically precipitated during peatification and/or early diagenetic stages, with a lesser extent of epigenetic precipitation during coalification (Table 6). Clay minerals are observed as matrices of clay mineral aggregates (Figure 9a-c), which are associated with quartz, feldspars, apatite, biotite, chlorite, pentlandite, sphalerite, Ti-oxide, and zircon grains, during petrographic and SEM-EDX studies.

Table 6: Syngenetically and epigenetically formed minerals identified using XRD and SEM-EDX in the coal and carbonaceous shale samples. Solid line indicates clearly identified minerals in the samples, dashed line shows possible identifications.

Çizelge 6: *XRD ve SEM-EDX yardımıyla incelenen kömür ve karbonlu şeyl örneklerindeki sinjenetik ve epijenetik olarak oluşan mineraller. Kesiksiz çizgiler tanımlanan minerallerin örneklerdeki ana kökenlerini ve kesikli çizgiler ise tanımlanan minerallerin olası kökenlerini işaret etmektedir.*

Minerals	Syngenetic		Epigenetic	
	Detritus	Authigenic precipitation in peat	Authigenic precipitation at depth	Authigenic weathering reactions
Quartz	———	- - - -	- - - -	
Clay minerals	———	- - - -		
Feldspars	———			
Biotite	———			
Zircon	———			
Calcite/Aragonite	- - - -	———		
Siderite		———		
Dolomite	- - - -			
Pyrite		———	- - - -	
Sphalerite	———			
Pentlandite	———			
Barite		———	- - - -	- - - -
Apatite	———	- - - -		
Ti-oxides	———			

The SEM-EDX data also show that the matrices of clay aggregates are mainly illitic and smectite compositions. Ilitic clay mineral aggregates in coals are generally related to clastic influx into paleomires from adjacent areas (Oskay et al., 2016; Ward, 2002), while clay mineral aggregates with smectite composition could be related to alteration of synchronous and/or epiclastic volcanic inputs due to the presence of tuffite layers within the Oligocene formations in the study area (Dai et al., 2017; Karayiğit et al., 2017; Spears, 2012). The existence of quartz, feldspars, biotite, Ti-oxide, and zircon grains within such matrices may also be an indicator of synchronous and/or epiclastic volcanic inputs into palaeomires (Bohor and Triplehorn, 1993; Dai et al., 2017). Nevertheless, these aggregates could also be

derived from the alteration of clastic influx from the basement. The existence of Fe-rich chlorite grains (chamosite) with lath shapes (Figure 9b) could suggest that these grains could be derived from the alteration of detrital inputs from the basement rocks within palaeomires. Overall, clay minerals in the Seam-VI seem to be mainly derived as clastic influx into paleomires, with a lesser extent of authigenic formation during peat accumulation and/or late stages of peatification.

Quartz/silica is mostly identified as individual grains and/or associated with clay minerals aggregates (Figure 9c-d). Considering the presence of tuffite layers in the Oligocene formations in the basin and the presence of metamorphic rocks in the basement, it can be concluded that quartz/silica grains have a detrital origin (Ward, 2016). Furthermore, quartz/silica cavity and cell-infillings within telohuminite macerals and cleat/fracture quartz/silica infillings were rarely observed in the studied samples. The former quartz/silica infillings could be related to re-precipitation of liberated Si from plant decay or the alteration of clastic inputs within palaeomires and/or early diagenetic stages (Ward, 2002); on the other hand, cleat/fracture quartz/silica infillings could originate from precipitation of Si-rich porewater and/or leached solutions from overlying sandstone layers within the Danişmen Formation during late diagenesis/coalification. Like quartz/silica, feldspar grains (plagioclase and K-feldspars) are observed either as individual grains or within clay mineral aggregates. The variable size and irregular edges of feldspar grains (Figure 9e-f) could imply that these grains are derived by clastic influx into the palaeomire from different sources (Dai et al., 2017; Karayiğit et al., 2022c). For instance, the presence of zircon within the cavities of feldspar grains (Figure 9f) could be derived from tuffite layers within the Oligocene formations; nevertheless, the presence of barite overgrowths around feldspar grains could suggest that these grains were altered within the palaeomires (Çelik et al., 2021).

Carbonate minerals in coal samples are mostly observed as carbonate mineral bands (Figure 10a-c) and rarely as individual grains within clay mineral aggregates. Furthermore, fossil shell remains in $CaCO_3$ compositions were identified in the samples bearing fossil shell remains (Figure 10d-e) as well as in siderite micronodules (Figure 10f). It is well documented from the Turkish Cenozoic coals that Ca-rich alkaline aquifer support into palaeomires resulted in the formation of authigenic carbonate mineral bands and siderite micronodules during peatification and/or early diagenetic stages (Karayiğit et al., 2017, 2022b, 2022c; Kortenski, 1992). Such conditions could also cause the formation of alkaline conditions within the palaeomire. Siderite micronodules in coal are generally considered evidence for low sulphur contents in the palaeomire (Dai et al., 2020a; Shen et al., 2023); however, the presence of pyrite and syngenetic carbonate-pyrite associations (Figure 10c) in the same samples could suggest that dissolved Fe might be high in mire water and/or weak acidic to neutral conditions were developed during the peat accumulation (Karayiğit et al., 2017, 2022b, 2022c; Ward, 2016). As noted earlier from other coal mining areas in the Malkara coalfield (Karayiğit et al., 2022a), the co-occurrence of pyrite and syngenetic carbonate minerals could indicate the formation of weak acidic to neutral conditions. It is noteworthy to mention that no replacement carbonates were observed in the Seam-VI, like other seams in the Malkara coalfield, which indicates dissolved Ca concentrations in the paleomires of Seam-VI were not high as in the palaeomires of other

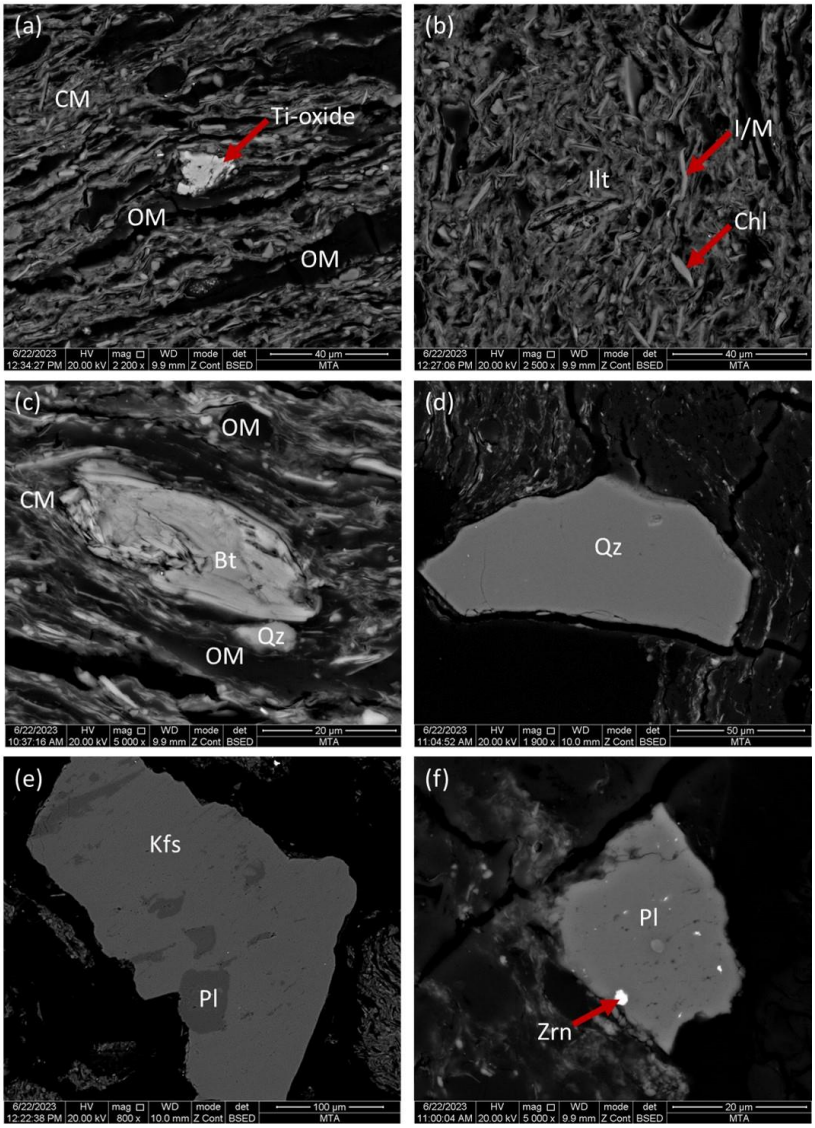

Figure 9: SEM backscattered images of crystalline phases in the studied coal and shale samples. (a-c) biotite (Bt), chlorite (Chl), illite/mica (I/M), Ti-oxide and quartz (Qz) grains associated with clay mineral (CM) matrix (illite: Ilt), and organic matter (OM); (d) individual quartz (Qz) grain; (e) plagioclase (Pl) associated with K-feldspar (Kfs) grain; (f) zircon (Zrn) within the cavities of plagioclase (Pl) grain.

Şekil 9: *İncelenen kömür ve şeyl örneklerdeki kristalin fazlara ait SEM geri saçılım görüntüleri. (a-c) kil mineralleri içerisindeki biyotit (Bt), illit/mika (I/M), klorit (Chl), kuvars (Qz) ve Ti-oksit taneleri ile organik madde (OM); (d) tekli kuvars (Qz) tanesi; (e) K-feldspat (Kfs) ile beraber gözlenen plajiyoklaz (Pl) tanesi; (f) plajiyoklaz (Pl) tanesi içerisindeki boşlukları içerisindeki zirkon (Zrn).*

seams in the Malkara coalfield. In addition, an increased Ca concentration and water level might also allow biogenic activities within the palaeomires (Ward, 2002); hence, calcareous shell remains are observed towards the upper parts of the Seam-VI.

Pyrite is the only identified sulphide mineral by XRD, while accessory sulphide minerals like sphalerite and pentlandite are detected during SEM studies (Table 6). The framboidal pyrite grains are the most common morphology, and partially pyritized calcareous fossil remains and cleat/fracture pyrite infillings are also observed in the samples (Figure 11a-c). The common presence of framboidal pyrite grains in coal seams is related to either marine influence into palaeomires and/or anoxic conditions within the palaeomires (Chou, 2012; Querol et al., 1989; Ward, 2016). The first possibly could not be applicable for the studied Seam-VI, since the detailed paleontological studies from the Malkara coalfield reported that the sequences bearing Seam-VI were deposited under flood plain and freshwater lakes (İslamoğlu et al., 2010; Şafak, 2019). Therefore, the development of anoxia seems to allow sulphate-reducing bacterial activity within the palaeomires (Chou, 2012). The formation of syngenetic framboidal pyrite grains could take place between pH 5.0 and 7.5 (Altschuler et al., 1983; Querol et al., 1989). As mentioned previously, the co-occurrence of pyrite and carbonate minerals implies that very weak acidic to neutral conditions were common dur ing the peat accumulation. Apart from syngenetic pyrite grains, the partially pyritized calcareous fossil remains (Figure 10d-e) and cleat/fracture pyrite infillings (Figure 6f) could be formed from the replacement of carbonates by S-rich porewater and precipitation from S-rich solutions within cleat/fractures during the late diagenetic stage or coalification.

Sphalerite and pentlandite grains have been identified within the clay mineral aggregates in the samples (Figures 12 and 13). Hence, the detritus origin for these sulphide minerals could be pronounced. The occurrence of pentlandite, along with chromite, in Turkish Cenozoic coals is mostly documented in the coalfields (e.g., Orhaneli and Tunçbilek) situated near ophiolitic rocks bearing Cr- and Ni- ore deposits (Karayiğit et al., 2019, 2021). On the contrary, no Cr- and Ni-ore deposits or mineralization were reported to date from ophiolitic rocks in the south-western parts of the Thrace Basin. Besides, sulphur mineralization and sulphide ore deposits were also reported from the Strandja and Rhodope massifs (Marchev et al., 2005; Mortiz et al., 2014; Taner and Çağatay, 1983). Considering the presence of pentlandite and sphalerite in these sulphide deposits, sphalerite and pentlandite in the samples are presumably derived from clastic influx into palaeomires from the Strandja and Rhodope massifs.

Barite and (Ba, Sr)-sulphates are the only identified sulphate minerals in the samples during the SEM studies (Table 6). They are commonly observed as overgrowth around the feldspar (Figures 11d and 14a) and or biotite grains (Figure 15a) and rarely as cleat/fracture infillings (Figure 11c). The barite overgrowths around feldspar or biotite grains could be related to the alteration of such grains within the palaeomires, and liberated Ba and Sr seem to be reduced by bacteria within the palaeomires (Çelik et al., 2021). Cleat/fracture barite infillings could be precipitated from Ba-bearing porewaters and/or leached solutions from the overlying sediments during coalification or post-coalification (Çelik et al., 2021; Dawson et al., 2012; Ward, 2016). Apatite is observed as individual grains within the clay minerals, which indicates a detritus

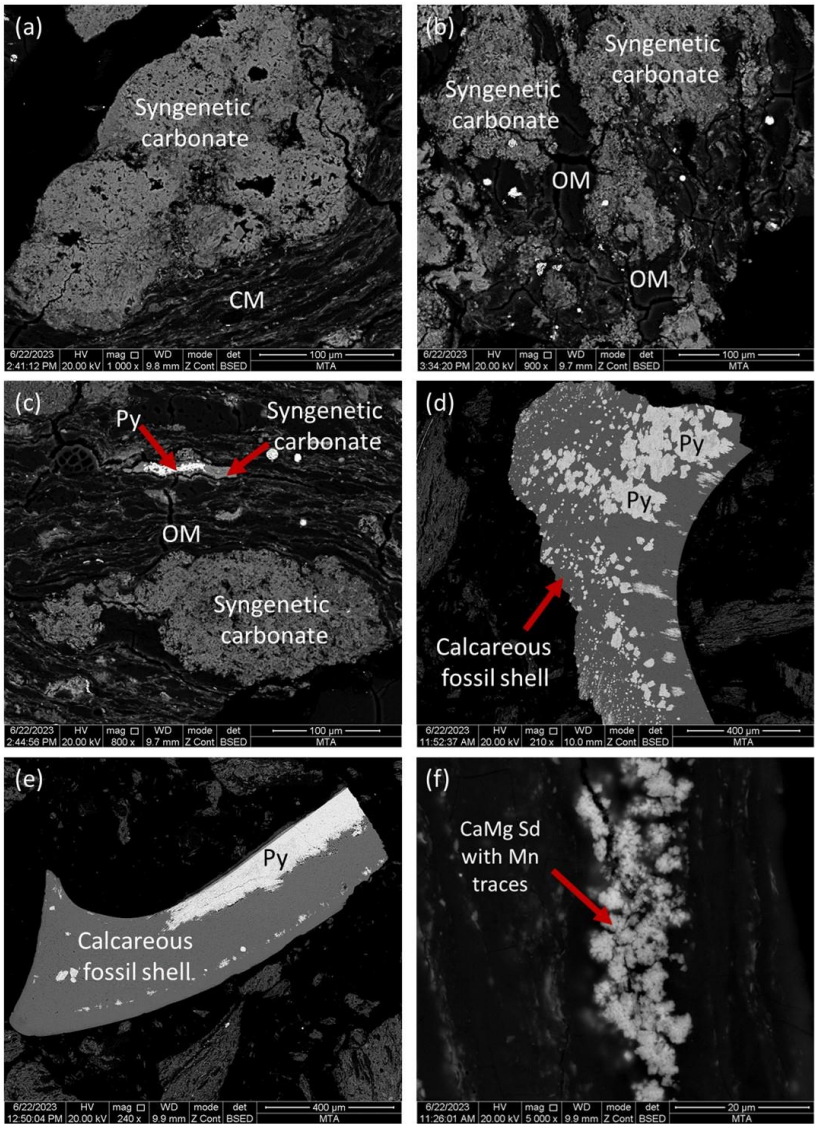

Figure 10: SEM backscattered images of crystalline phases in the studied coal and shale samples. (a-c) sygenetic carbonate mineral bands associated with organic matter (OM) and pyrite (Py), and clay minerals (CM); (d-e) partially pyritized (Py) calcareous fossil shell remains; (f) CaMg-siderite (Sd) micronodules with measurable Mn.

Şekil 10: *İncelenen kömür ve şeyl örneklerdeki kristalin fazlara ait SEM geri saçılım görüntüleri. (a-c) organik madde (OM) ile beraber gözlenen sinjenetik karbonat mineral bantları ile pirit (Py) ve kil mineralleri (CM); (d-e) kısmen piritleşmiş (Py) kalkerli fosil kavkı kalıntıları; (f) ölçülebilir miktarda Mn içeren CaMg-siderit nodülü.*

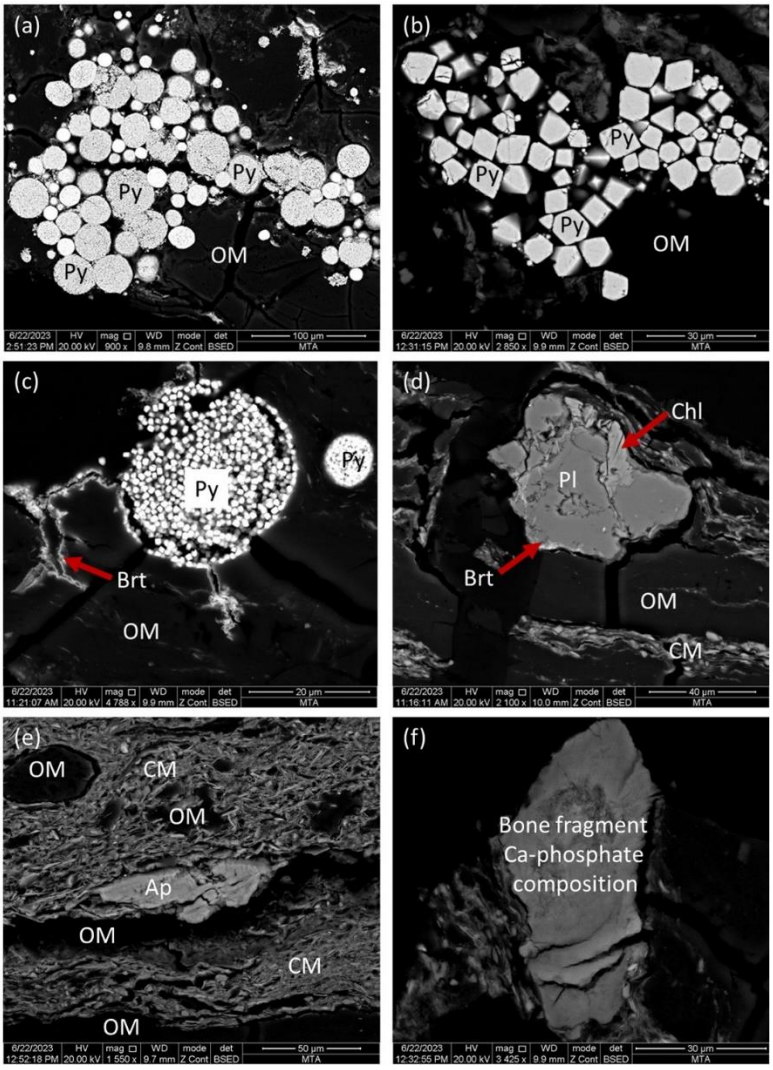

Figure 11: SEM backscattered images of crystalline phases in the studied coal and shale samples. (a) framboidal pyrite (Py) grains within organic matter (OM); (b) euhedral pyrite (Py) within organic matter (OM); (c) framboidal pyrite (Py) grains within organic matter, and cleat/fracture barite (Brt); (d) barite (Brt) overgrowths around plagioclase (Pl) grain, and chlorite (Chl), clay minerals (CM) and organic matter (OM); (e) apatite (Ap) associated with clay mineral (CM) aggregates, and organic matter (OM); (f) fossil bone fragment with Ca-phosphate composition.

Şekil 11: *İncelenen kömür ve şeyl örneklerdeki kristalin fazlara ait SEM geri saçılım görüntüleri. (a) organik madde (OM) içerisindeki framboidal piritler (Py); (b) organik madde (OM) içerisindeki özşekilli piritler (Py); (c) organik madde (OM) içerisindeki framboidal piritler (Py) ve kırık/çatlak dolgusu barit (Brt); (d) plajiyoklaz (Pl) tanesi etrafındaki barit (Brt) büyümleri, kil minerali (CM), klorit (Chl) ve organik madde (OM); (f) Ca-fosfat bileşimli fosil kemik kalıntısı.*

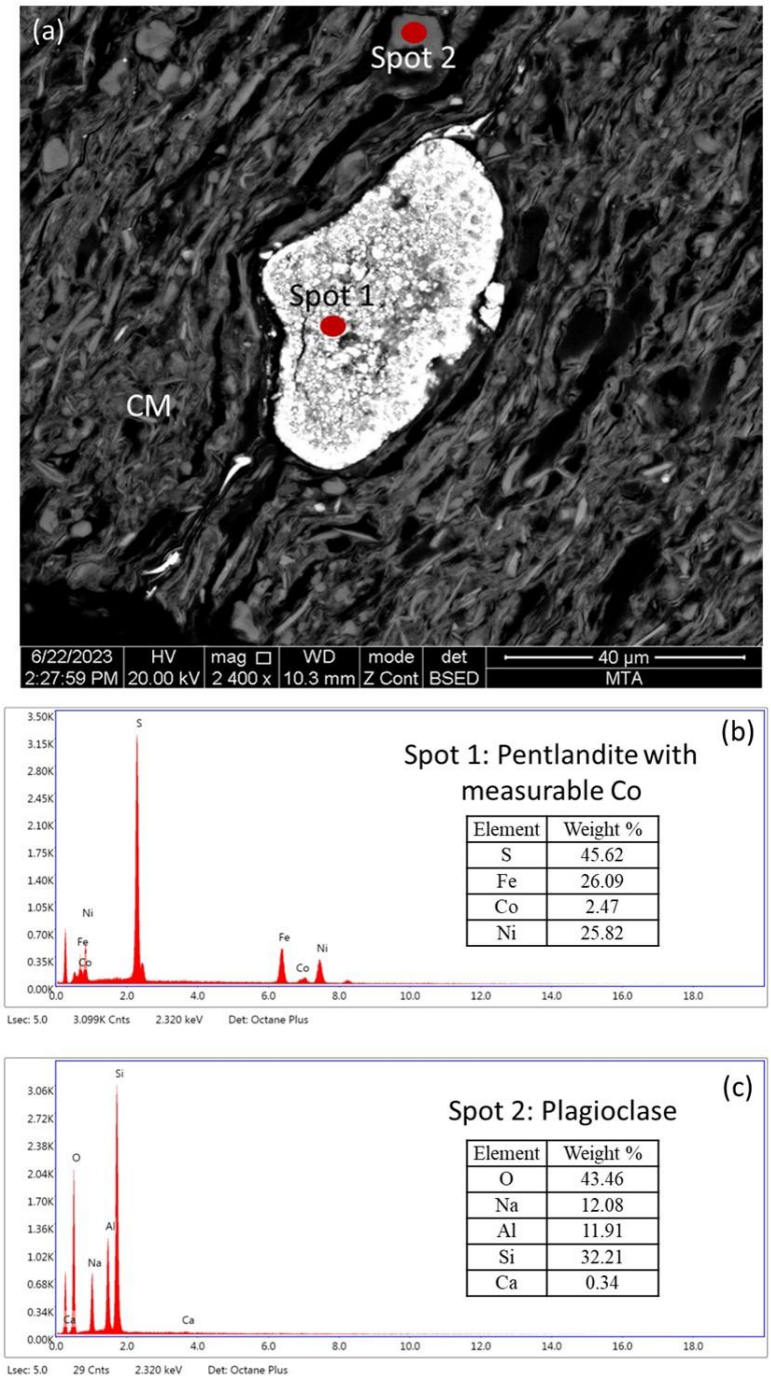

Figure 12: (a) SEM backscattered image of pentlandite and plagioclase grains associated with clay mineral (CM) aggregates; SEM-EDX spectra of (b) pentlandite at spot-1 and (c) plagioclase at spot-2.

Şekil 12: *Kil minerali (CM) yığışımları içerisindeki pentlandit ve plajiyoklaz tanelerine ait SEM geri saçılım görüntüsü. (b) Spot-1'deki pentlandit ve (c) Spot-2'deki plajiyoklaz ait SEM-EDX spektraları.*

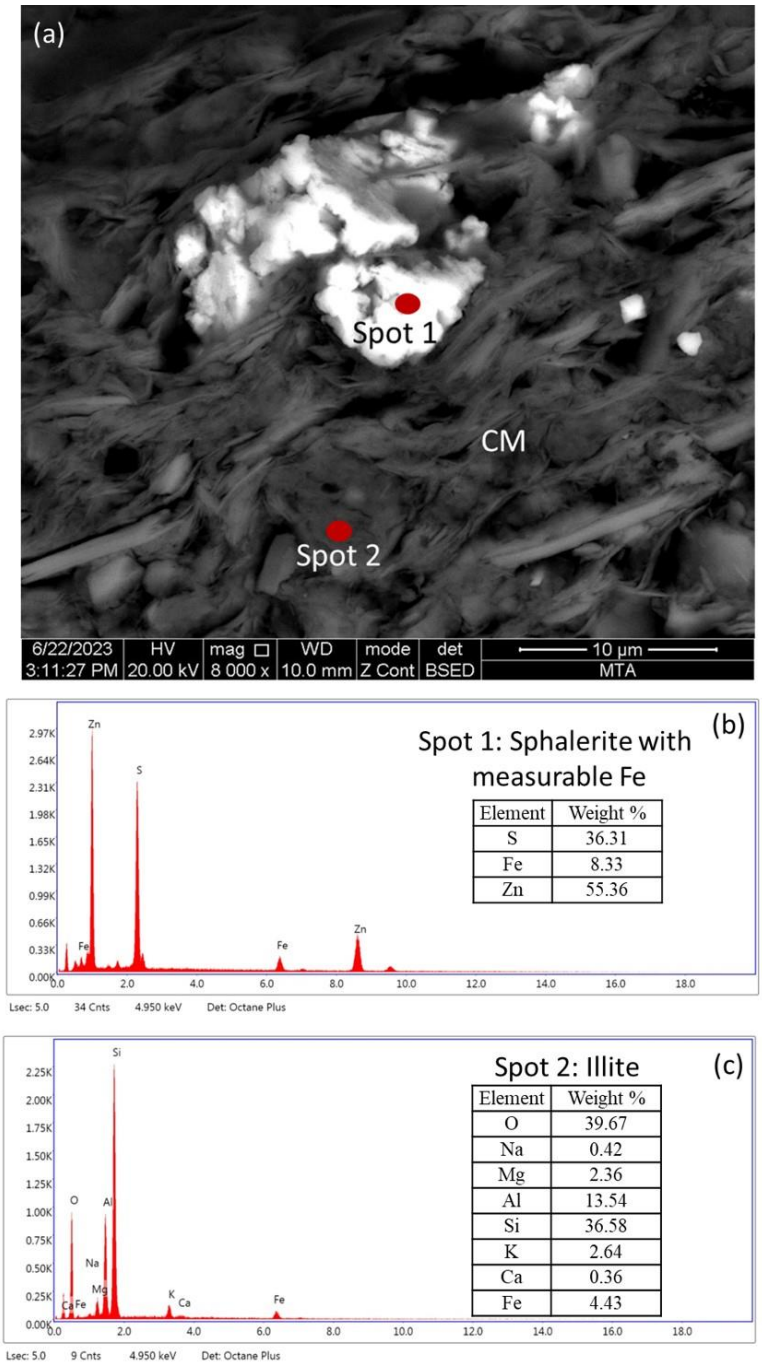

Figure 13: (a) SEM backscattered image of sphalerite grains associated with clay mineral (CM) aggregates (illite); SEM-EDX spectra of (b) sphalerite at spot-1 and (c) illite at spot-2.

Şekil 13: *Kil minerali (CM) yığışımları içerisindeki sfalerit tanelerine ait SEM geri saçılım görüntüsü. (b) Spot-1'deki sfalerit ve (c) Spot-2'deki illite ait SEM-EDX spektraları.*

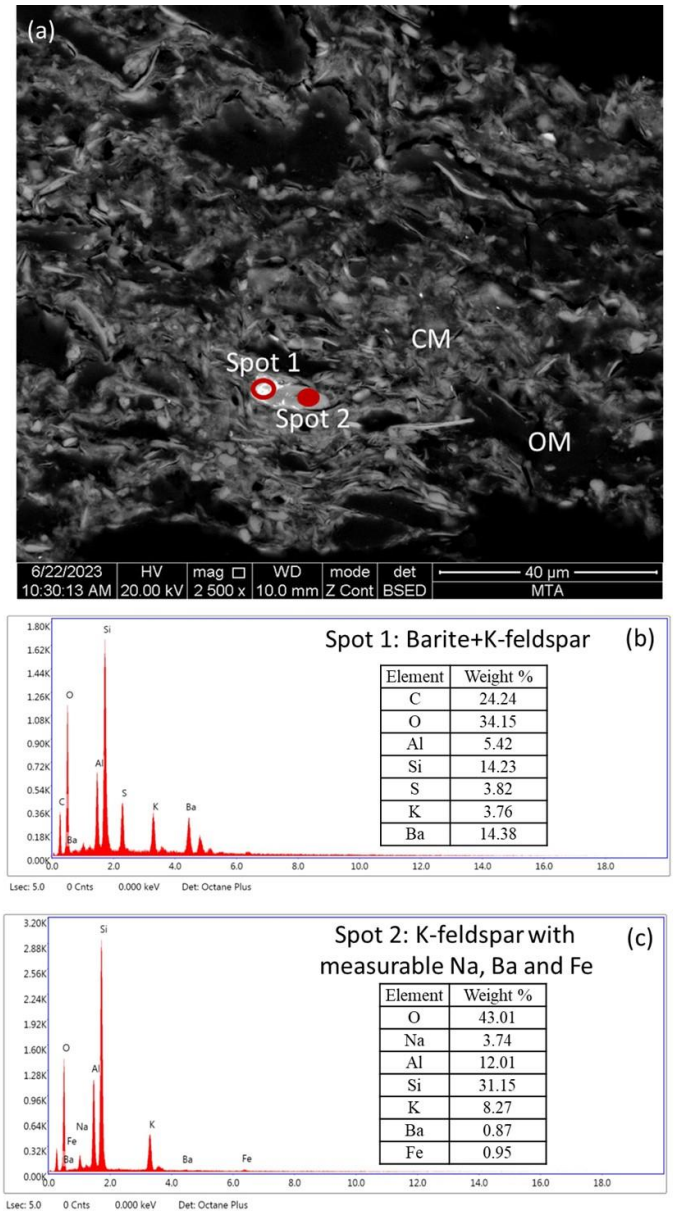

Figure 14: (a) SEM backscattered image of barite (Brt) overgrowth around K-feldspar (Kfs) grain associated with clay mineral (CM) aggregates, and organic matter (OM); SEM-EDX spectra of (b) barite and K-feldspars at spot-1 and (c) K-feldpsar at spot-2.

Şekil 14: *Kil minerali (CM) yığışımları içerisindeki K-feldspat etrafında gelişen barit büyümleri ve organik maddeye (OM) ait SEM geri saçılım görüntüsü. (b) Spot-1'deki barit+K-feldspat ve (c) Spot-2'deki K-feldspata ait SEM-EDX spektraları.*

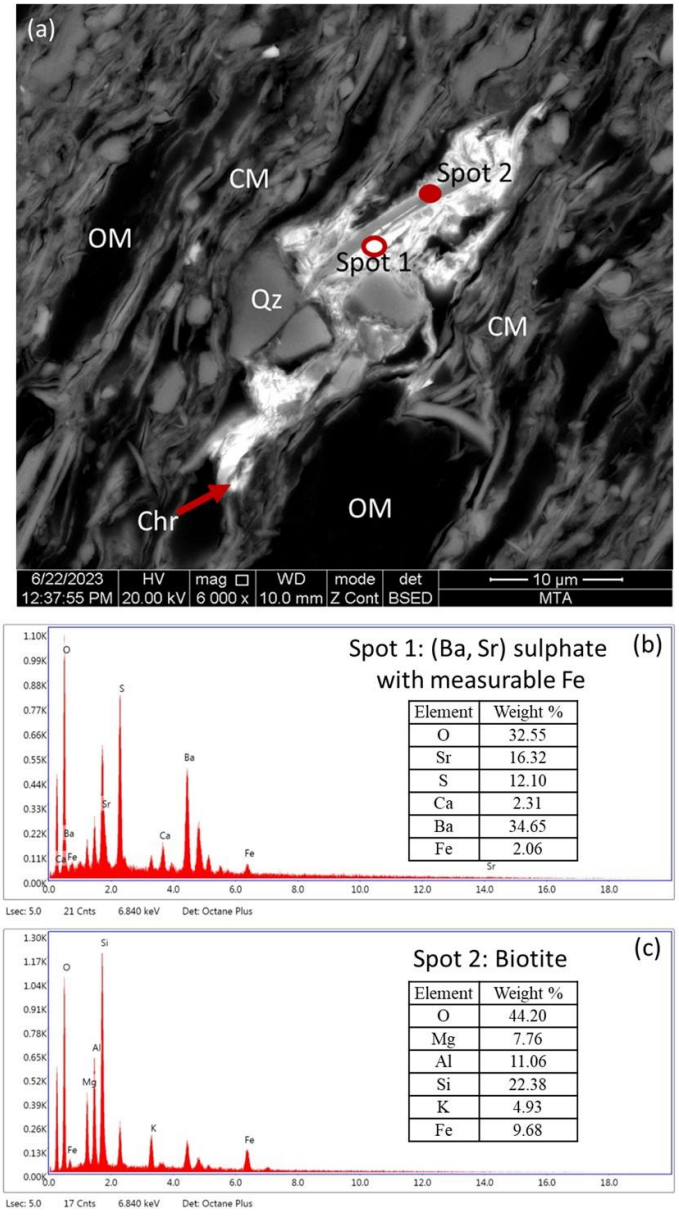

Figure 15: (a) SEM backscattered image of (Ba,Sr)-sulphate overgrowth around biotite grain, chromite (Chr) and quartz (Qz) grains associated with clay mineral (CM) aggregates, and organic matter (OM); SEM-EDX spectra of (b) (Ba,Sr)-sulphate at spot-1 and (c) biotite at spot-2.

Şekil 15: *Kil minerali (CM) yığışımları içerisindeki biyotit etrafında gelişen (Ba,Sr)-sülfat büyümeleri, kromit (Chr) ve kuvars (Qz) tanelerine ait SEM geri saçılım görüntüsü. (b) Spot-1'deki Ba,Sr)-sülfat ve (c) Spot-2'deki biyotite ait SEM-EDX spektraları.*

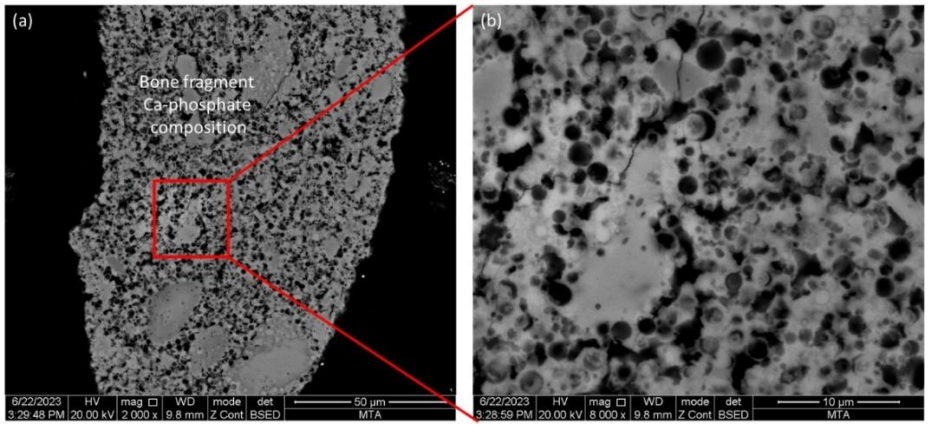

Figure 16: (a) SEM backscattered image of fossil bone fragment with Ca-phosphate composition; (b) enlarged view of selected area in image a.

Şekil 16: *(a) Ca-fosfat bileşimli fosil kemik kalıntısına ait SEM geri saçılım görüntüsü ve (b) Şekil 16a'daki seçili alanın büyütülmüş görüntüsü.*

origin (Ward, 2016); nevertheless, fossil bone remains with Ca-phosphate compositions were also detected during the SEM studies (Figures 11f and 16). Like calcareous fossil shell remains, these remains could also be indicators of increased biogenic activities within the palaeomires (Ward, 2002). Even though it is not easy to identify the origins of these bone remains, their co-occurrence with calcareous fossil shell remains may be related to the presence of aquatic animals due to increased water levels within the palaeomires.

Mode of occurrence of elements and elemental enrichments

The mode of occurrence of certain elements in coal could also be a useful tool for estimating depositional conditions during peat accumulation and/or the chemistry of porewater and circulating fluids within coal beds (Dai et al., 2020a, b; Finkelman et al., 2019). For this purpose, statistical methods (e.g., Pearson correlation or hierarchical cluster) have been commonly applied; however, recent studies show that statistical methods should be combined with direct methods, such as SEM-EDX or EPMA, in order to eliminate inaccurate correlations among elements (Eminağaoğlu et al., 2022; Eskanazy et al., 2010; Xu et al., 2020, 2022, 2023). Therefore, we combine statistical data with SEM-EDX data in this study in order to have results that are more robust.

Ash yields display strongly positive correlations with SiO_2 (r_{ash}=+0.905), Al_2O_3 (r_{ash}=+0.763), and K_2O (r_{ash}=+0.788), whereas they exhibit weak to moderately negative correlations with CaO (r_{ash}=-0.518), Fe_2O_3 (r_{ash}=-0.658), MgO (r_{ash}=-0.433), and Na_2O (r_{ash}=-0.518). These correlations could indicate that the concentrations of SiO_2, Al_2O_3, and K_2O in the samples are controlled by mineral matter. Since clay minerals, particularly illite and smectite, are the dominant phases, and quartz is abundantly present in the samples, SiO_2 and Al_2O_3 could be affiliated with clay minerals, and

SiO_2 is also associated with quartz. This assumption could also be supported by the SEM-EDX data, and K is also traced from the illitic clay matrix (Figure 13c). Furthermore, Al_2O_3 and K_2O are also traced from feldspars and biotite grains in the samples (Figures 14b and 15c). Several trace elements, such as Li, Sc, Ni, Cu, Ti, and Zr, have meaningfully moderate positive correlations with Al_2O_3 and SiO_2, which imply aluminosilicate affinity (Table 7). Besides, some of these elements are also affiliated with accessory minerals (e.g., biotite, Ti-oxide, and zircon) in the samples.

Table 7: Element affinities with ash yield and total S (%,db) deduced from the calculation of Pearson's correlation coefficients (**: correlation in table is significant at 0.01 level, 2-tailed, *: correlation is significant at 0.05 level, 2-tailed, x otherwise indicates correlation is less significant lower 0.05 level, 2-tailed).

Çizelge 7: *Pearson korelasyon katsayısı hesaplanmasına göre kül ve toplam S (%, db) içerikleri ile elementlerin ilişkileri (**: korelasyon 0,01 düzeyinde anlamlı, 2 kuyruklu, *: korelasyon 0,05 düzeyinde anlamlı, 2 kuyruklu, x aksi halde korelasyonun 0,05 düzeyinden düşük, 2 kuyruklu olduğunu gösterir).*

Correlation with ash content 0.70<r<1.0
SiO_2**, Al_2O_3*, K_2O**, Cr**, Ni**, Cu**, Zn**, Ge*, Pb**
Correlation with ash content 0.40<r<0.70
P^x, V*, Mo^x, Co*
Correlation with ash content r>-0.40
Total S^x, Na_2O^x, MgO^x, CaO^x, Fe_2O_3*, B**, Be^x, Ba^x
Correlation with SiO_2 content 0.40<r<1.0
TiO_2^x, Al_2O_3**, K_2O**, Li*, Sc*, V**, Cr**, Co**, Ni**, Cu**, Zn**, Ge*, Nb^x, Mo**, Pb**
Correlation with Al_2O_3 content 0.40<r<1.0
TiO_2*, SiO_2**, K_2O**, Li*, Sc*, V**, Cr**, Co**, Ni**, Cu**, Zn**, Ge*, Zr^x, Nb*, Mo**, Pb**
Correlation with CaO content 0.40<r<1.0
Total S^x, As^x, Sr**, Ba^x
Correlation with total S content 0.40<r<1.0
Fe_2O_3**, CaO^x, B*, As^x, Sr*, Ba*

The negative correlations among ash yields, Fe_2O_3, MgO, and Na_2O could indicate organic affinities for these major oxides (Table 7), and Fe, Mg, and Na could be incorporated with organic matter in coal (Dai et al., 2020b). Fe_2O_3 also displays a positive correlation with total S contents (Table 7), which implies sulphide affinity for Fe, and additionally, SEM-EDX data also show that Fe is traced from pyrite, clay minerals (illitic matrix and chlorite grains), and accessory minerals, such as pentlandite, sphalerite, and barite (Figures 12b, 13b-c, 14b-c and 15b-c). This data implies that Fe_2O_3 seems to have mainly inorganic affinity instead of organic affinity. Pyrite is generally an abundant phase in the xylite-rich lithotype coal samples, and these samples have relatively lower ash yields (Table 1). Therefore, pseudo-correlations between ash yield and Fe_2O_3 are developed. Additionally, MgO is also traced from clay minerals, particularly smectite aggregates, chlorite grains (Figures 13c and 15c), and clay minerals and feldspar grains also contain measurable amount of Na by SEM-EDX (Figures 12c, 13c and14c). Hence, MgO and Na_2O may also have aluminosilicate

affinity. Overall, SiO_2, Al_2O_3, K_2O, MgO, and Na_2O are mainly affiliated with aluminosilicate minerals, while Fe_2O_3 is mainly associated with sulphide minerals and, to a lesser extent, aluminosilicate minerals.

The negative correlations between ash and CaO could be an indicator of organic affinity (Table 7), and the existence of measurable amounts of Ca from organic matter by SEM-EDX could be testimony to this assumption. This could be related to Ca uptake by peat-forming plants from Ca-rich mire water and/or non-mineral Ca in the organic matter (Dai et al., 2020b; Karayiğit et al., 2017, 2021). Nevertheless, the presence of syngenetic carbonate mineral bands, calcareous fossil shell remains and siderite micronodules (Figures 10a-f and 17a-b) in the upper parts of Seam-VI could indicate that CaO has also inorganic affinity. Thus, Ca-rich water support into palaeomires and the development of weak acidic to neutral conditions within the palaeomires could control CaO concentrations of the samples. Moreover, apatite, barite, and feldspar grains and fossil bone remains in Ca-phosphate compositions serve as other other inorganic sources for CaO. Interestingly, biogenic activities within palaeomires might also cause elevations of CaO concentrations as fossil bone and calcareous shell remains-bearing samples have relatively higher CaO concentrations. All these imply that CaO exhibits dual affinity, and water chemistry and biogenic activities within the palaeomires may control CaO concentrations of the Seam-VI.

Boron enrichments in the Turkish Cenozoic coals are commonly reported, and B is mostly associated with clay minerals, organic matter, and possible accessory presences of B-bearing silicate minerals (e.g., tourmaline and zeolite minerals) (Çelik et al., 2021; Karayiğit et al., 2020a; Palmer et al., 2004). In the samples, B has meaningful negative correlations with ash yields (Table 7), which suggests an organic affinity for B in the studied samples. Furthermore, the dominance of clay minerals in the studied samples and the accessory presence of biotite could be other sources for B in the samples. Although B seems to have mainly organic affinity, the source of B-rich mire water is another question that should be addressed. Like the studied Seam-VI, B enrichments are also reported from the coal seams within the Danişmen Formation (Çelik et al., 2017; Güllüdağ and Altunsoy, 2022; Tuncalı et al., 2002). Since transgressive and regressive events took place during the Oligocene in the Thrace Basin (Batı and Gürgey, 2018), B enrichments in coal seams within the Danişmen Formation could be

controlled by seawater penetration into palaeomires and/or after peatification. This assumption could be supported by B concentrations higher than 100 ppm, and the mean %Rr values are 0.40-0.41% (Dai et al., 2020a; Goodarzi and Swaine, 1994); however, B concentrations higher than 100 ppm could also be reported from coal seams within pure limnic sequences (Karayiğit et al., 2017). In agreement, coal seams within floodplain deposits in the Thrace Basin display relatively high B concentrations (Çelik et al., 2017). As mentioned above, the sequences bearing Seam-VI were deposited under floodplain and freshwater lake conditions (İslamoğlu et al., 2010); hence, B enrichments in the Seam-VI might not be controlled by seawater influence into palaeomire or post-peatification. Boron enrichments in coal seams within fluvio-lacustrine sequences in the Turkish Cenozoic coals are generally controlled by uptake B by peat-forming plants from B-rich leached surface water from volcanic/volcanoclastic rocks and/or synchronous and/or epiclastic volcanic inputs into palaeomires (Karayiğit et

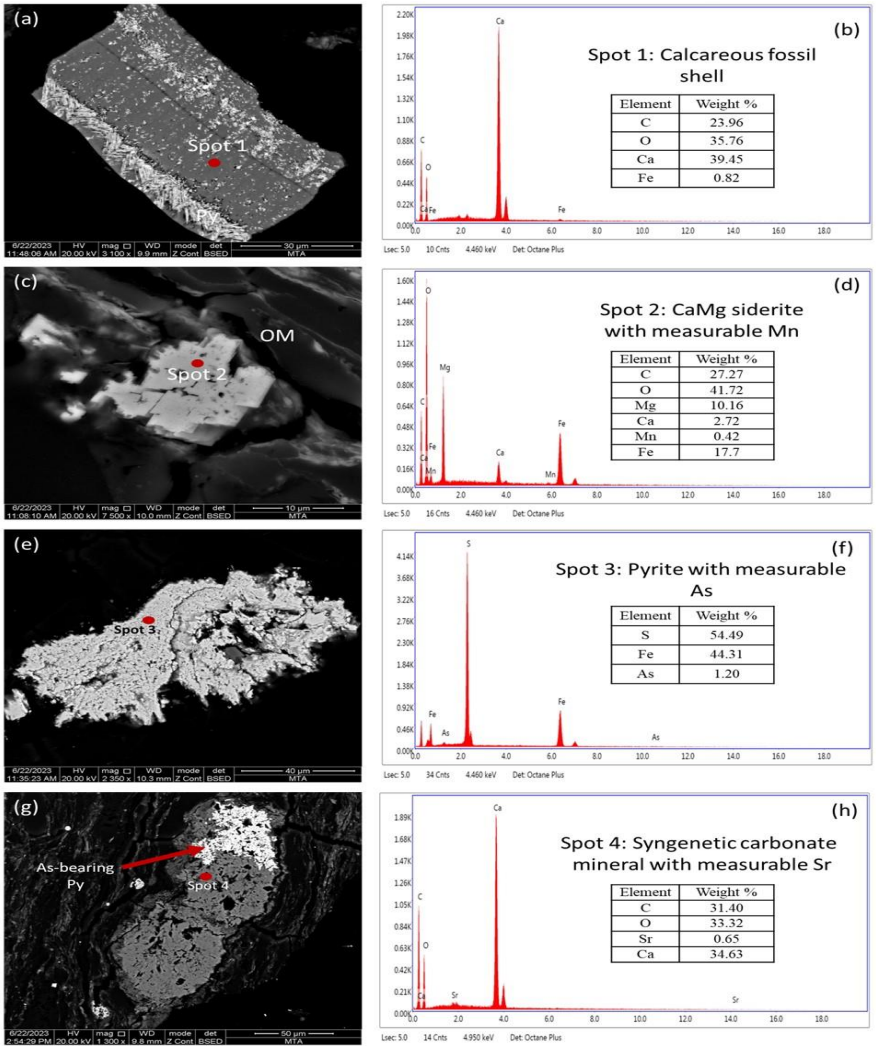

Figure 17: SEM backscattered images of crystalline phases in the studied coal and shale samples. (a) partially pyritized (Py) calcareous fossil shell remain; (b) SEM-EDX spectra of calcareous fossil shell remain at spot-1; (c) siderite micronodule within organic matter (OM); (d) SEM-EDX spectra of CaMg-siderite micronodule at spot-2; (e) pyrite grain; (f) SEM-EDX spectra of pyrite with measurable As at spot-3; (g) syngenetic carbonate mineral band associated with As-bearing pyrite (Py); (h) SEM-EDX spectra of syngenetic carbonate mineral band with measurable Sr at spot-4.

Şekil 17: *İncelenen kömür ve şeyl örneklerdeki kristalin fazlara ait SEM geri saçılım görüntüleri. (a) kısmen piritleşmiş (Py) kalkerli fosil kavkı kalıntısı; (b) spot-1'deki kalkerli fosil kavkı kalıntısına ait SEM-EDX spektrası; (c) organik madde (OM) içerisindeki siderite mikronodülü; (d) spot-2'deki CaMg-siderit nodülüne ait SEM-EDX spektrası; (e) pirit; (f) spot-3'deki As içeren pirite ait SEM-EDX spektrası; (g) As içeren pirit ile beraber bulunan sinjenetik carbonate minerali bandı; (h) spot-4'teki Sr içeren sinjenetik karbonat minerali bandına ait SEM-EDX spektrası.*

al., 2017, 2022a; Querol et al., 1997). This scenario might also be possible for the studied Seam-VI due to the presence of tuffite layers within the Oligocene sequences in the Thrace Basin. Thus, B-enrichments in the samples are mainly controlled by epiclastic influx from Oligocene tuffite layers into palaeomire, and liberated B from the alteration of epiclastic material seems to be taken by peat-forming plants.

Manganese in coal is mainly affiliated with carbonate minerals, particularly siderite and calcite, as well as Fe-sulphide minerals (e.g., pyrite) (Dai et al., 2021; Finkelman et al., 2019). Manganese -bearing siderite micronodules have been identified by SEM-EDX in the extremely high Mn-bearing sample 18-13/03 (Figures 10f and 17b). Such siderite micronodules could be an indicator of seawater influence (Antoshkina et al., 2017; Mozley, 1989); however, it is also documented that Mn-bearing siderite micronodules could be deposited under freshwater conditions due to the development of weak acidic to neutral conditions within palaeomires and/or during the late stages of peatification (Karayiğit et al., 2017, 2022a; Passey, 2014; Shang et al., 2023). In such cases, Mn could be derived from either the dissolution of synchronous and/or epiclastic volcanic inputs or Mn-rich surface water leached from magmatic rocks or marine carbonates. Hence, mire water could be enriched with Mn^{2+}, and Mn^{2+} could be substituted with Fe^{2+} in siderite micronodules. Considering the presence of Eocene marine carbonates, Mn mineralizations and Mn-deposits within the early Oligocene sequences (Gürgey and Batı, 2018; Gültekin, 1998, 1999; Gültekin and Balcı, 2018), the peat-forming environment in the study area had sufficient amounts of dissolved Fe^{2+} and Mn^{2+} ions within mire water and/or porewater during the late peatification stages. Thus, the formation of Mn-bearing siderite micronodules control Mn enrichments in the Seam-VI.

Nickel in coal is generally affiliated with sulphide minerals and clay minerals (Dai et al., 2021; Finkelman et al., 2019; Ruppert et al., 1996). Nickel displays meaningfully strong positive correlations with ash yields, Al_2O_3 and SiO_2 (Table 7), which indicates aluminosilicate affinity. Similar correlations were generally reported in Turkish Cenozoic coals (Palmer et al., 2004); on the other hand, the SEM-EDX data from these coals generally provide sulphide affinity (e.g., pyrite and pentlandite) instead of aluminosilicate affinity (Karayiğit et al., 2019, 2021, 2020). Of note, Ni-bearing sulphide mineral grains, particularly pentlandite, have been observed within the clay mineral matrix, and the source of pentlandite grains is generally related to clastic influx from Ni ore-bearing basement rocks. Even though Ni2+ could be substituted with Fe2+ in clay minerals (e.g., chlorite), the existence of such detritus Ni-sulphide mineral grains within clay minerals matrix could cause the correlations between Ni, Al2O3, and SiO2. More interestingly, Ni displays a negative correlation with the total S contents of the samples. This negative correlation could easily indicate that Ni is not affiliated with sulphide minerals; however, this correlation might be developed due to the relatively high total S contents of low ash yields xylite-rich lithotype samples. On the contrary, pentlandite grains are also commonly observed within clay mineral aggregates during SEM-EDX studies in the samples (Figure 12a-b). As mentioned earlier, these grains are presumably originated from clastic influx from sulphide mineralization and/or ores in the Strandja and/or Rhodope massifs (Marchev et al., 2005; Mortiz et al., 2014; Taner and Çağatay, 1983). Moreover, pentlandite grains in the samples also contain a measureable amount of Co by SEM-EDX

(Figure 12a-b). Nickel also shows moderate to positive correlations with Cu, Zn, and Pb (Table 7), which imply sulphide affinity for these elements. In agreement, detritus sphalerite grains are identified within clay mineral aggregates during SEM-EDX studies (Figure 13a-b). Therefore, as like Ni and Co, Cu, Zn and Pb concentrations in the samples might be controlled by the clastic influx into palaeomires from sulphide mineralisation and ore deposits in the Strandja and Rhodope massifs.

Like Ni, Cr and V also originate from clay minerals, sulphide minerals, and organic matter (Dai et al., 2021; Finkelman, 1994); however, detrital chromite grains, which originate from Cr- and Ni-bearing ore deposits, control their enrichments in Turkish Cenozoic coals (Karayiğit et al., 2019, 2020, 2021). Chromium and V display moderate to strong positive correlations with Al2O3, SiO2, Ni, and Co (Table 7). These correlations imply that both elements could be associated with either aluminosilicate minerals or Ni-bearing chromite grains in the samples. Notwithstanding that Karayiğit et al. (2022a) reported the accessory presence of detritus chromite grains from the coal seams within the Danişmen Formation, chromite grains have been detected in the studied samples from the Seam-VI in the İbrice area during SEM studies (Figure 15a). Nevertheless, both elements could substitute for Fe and Mg in clay minerals, particularly chlorites. Since chlorite grains are observed together with pentlandite grains within clay mineral aggregates in the samples through SEM studies, the correlations among Cr, V, Ni, and Co are presumably pseudo-correlations. Both chlorite and pentlandite grains have a detrital origin; in turn, Cr enrichments in the Seam-VI are presumably controlled by clastic influx into palaeomires.

Germanium in coal is mostly considered as an organically affiliated element, and its enrichment could be controlled by the existence of Ge-ore deposits and/or granitic rocks in the basement rocks and circulating hydrothermal solutions within coal seams (Dai et al., 2021; Yudovich, 2003). In contrast, Ge displays positive correlations with ash yields, Al2O3, and SiO2, and it does not have any meaningful correlations with maceral proportions. Therefore, the organic affinity might not be pronounced for Ge. According to general acceptance, Ge concentrations could be higher in the upper and lower parts and/or margins of coal deposits (Yudovich, 2003). Within this context, Ge could have relatively higher concentrations in the upper and lower parts of the sampling profile; however, Ge does not show any significant differences throughout the Seam-VI (Figure 8b). Besides, Ge also displays moderate positive correlations with Co, Ni, Cu, Zn, and Pb, which have mainly sulphide affinity. Even though Ge was not detected in sulphide minerals from the samples by used SEM equipment, it is reported that Ge-bearing sulphide minerals (e.g., sphalerite) could occur in sulphide deposits (Bernstein, 1985; Melcher et al., 2006; Yang et al., 2022). Since detritus sphalerite and pentlandite are observed in the samples during SEM-EDX analyses suggest a potential connection between Ge and the detritus sulphide mineral grains, which could originate from sulphide deposits in the basement. Although additional high-resolution (e.g., EPMA or TEM) analyses might be essential in the future, the correlation data among Ge, Ni, and Zn (Table 7) could imply that Ge enrichment in the Seam-VI could be controlled by clastic influx from sulphide ore-bearing deposits in the basement. The mode of occurrence of As in coal has been subjected to several studies due to its environmental

impacts. The results of these studies indicated that As in coal is mainly derived from sulphide minerals and organic matter, with rare occurrences in aluminosilicate minerals (Dai et al., 2021; Finkelman et al., 2002; Hower et al., 2017). In the samples, As concentrations are close to world low-rank coal averages; nevertheless, As has moderately positive correlations with the total S contents of the samples (Table 7). Thus, As seems to have a sulphide affinity. The SEM-EDX data also agrees with this assumption, and As is traced from pyrites associated with syngenetic carbonate mineral bands (Figure 17e-h). The source of As in pyrite could be dissolved As from leached surface water sulphur mineralisation and sulhpide ore deposits in the Strandja and Rhodope massifs. Anaerobic conditions during peatification may cause the formation of As-bearing pyrites; in turn, As concentrations in syngenetic carbonate mineral band-bearing samples are relatively higher than other samples (Figure 17c-d). This could also explain weak positive correlation between As and CaO contents (Table 7). Molybdenum is another element could be affiliated with organic matter and sulphide minerals in coal (Dai et al., 2021; Finkelman et al., 2018), and it could also be redox-sensitive element together with As (Querol et al., 1996). In the samples, Mo displays moderate positive correlations with ash yields and chalcophille elements, such as Ni, Cu, Zn and Pb (Table 7); however, it has negative correlations with total S and no meaningful correlation with As. All these factors could suggest that enrichment of Mo in the samples may not be controlled by redox conditions in the palaeomires or may not mainly affiliated with As-bearing pyrites in the samples. Even though the detection of Mo by SEM-EDX in the studied samples could be problematic due to its overlap with S, detritus sulphide minerals might be source of Mo in the samples. Cupper-Mo porphyry ore deposits are also located in the Strandja and Rhodope massifs (Gültekin, 1999; Mavrogonatos et al., 2018; Ohta et al., 1988). Overall, Mo enrichments in the Seam-VI could also be related to clastic influx originating from ore-bearing Strandja and Rhodope massifs.

Strontium and Ba in coal are generally affiliated with organic matter, Sr- and Ba-bearing sulphate minerals, carbonates, and phosphate minerals, with rare occurrences in aluminosilicate minerals (Çelik et al., 2021; Dai et al., 2021; Ward et al., 1996). The ratio of Sr/Ba could serve as an indicator of paleosalinity (Dai et al., 2020a; Spiro et al., 2019). The Sr/Ba ratio of all analysed samples is higher than 1.0. As discussed above, the studied Seam-VI was deposited under freshwater conditions; however, this ratio could not be an accurate parameter for palaeosalinity estimation due to the existence of accessory minerals containing Sr and Ba (e.g., barite, zeolites, or phosphates) or Sr-bearing syngenetic carbonate minerals (Çelik et al., 2021; Dai et al., 2020a; Karayiğit et al., 2022c). In the studied samples, Sr and Ba display weak to moderate positive correlations with CaO and total S contents (Table 7). These correlations could imply carbonate and sulphate affinity for both elements. Supporting this assumption, Ca- and Sr-bearing barite overgrowths are observed around feldspar grains, and K-feldspar grains contain measurable Ba as revealed by SEM-EDX (Figures 11e and 14a-b). Furthermore, (Sr, Ba)-sulphate overgrowths are also identified around biotite grains (Figure 15a-b). Therefore, Ba and Sr mainly exhibits sulphate affinity in the samples. In Turkish Cenozoic coals, the presence of Sr-bearing calcareous fossil shell remains have been reported (Karayiğit et al., 2000). Considering the calcareous fossil shell remains observed in the samples, carbonate affinity is expected for

Sr. The SEM-EDX data, on the other hand, show that these remains do not contain a measurable amount of Sr (Figure 17a-b). The lack of Sr in such remains could be attributed to the potential discharge of Sr from aragonitic shell remains during calcination (Marcano et al., 2015). The SEM-EDX data also shows that Sr is traced from the syngenetic carbonate mineral bands (Figure 17g-h). The Sr in these bands may originated from either release of Sr in aragonitic shell remains or liberated Sr resulting from alterations of feldspar and/or biotite grains. Both could be possible, and Sr2+ ions seem to be incorporated into syngenetic carbonate mineral bands due to the formation of weak acidic to neutral conditions in the palaeomires and/or during the peatification.

Coal facies

The analysis of coal facies could be useful tools for estimating conditions during peat accumulation (Diesel, 1992; Calder et al., 1991; Kalaitzidis et al., 2004; Tuncer et al., 2023). The origins of some inertinite macerals or possible allochthonous origins of some liptinite (e.g., sporinite) and inertinite (e.g., inertodetrinite) macerals could cause misinterpretations (Crosdale, 1993; Dai et al., 2020a; O'Keefe et al., 2013; Scott, 2002). To overcome this problem and to make more accurate assumptions, coal facies analyses should be correlated with several parameters, i.e., palynofloral assemblages, sedimentological, geochemical, and mineralogical data obtained from coal seams and coal-bearing sequences (Bechtel et al., 2004; Çelik et al., 2021; Oskay et al., 2016, 2019; Zieger and Littke, 2019; Zdravkov et al., 2017, 2020). As a traditional approach, the plotting of data on a ternary diagram (Figure 18), which was designed by Mukhopadhyay (1989), implies that woody peat-forming vegetation was common in the palaeomires of the Seam-VI, and the contribution of herbaceous peat-forming plants (e.g., reeds) seems to be increased occasionally (Figure 18). Additionally, anoxic conditions might be common during peat accumulation, which could be supported by the presence of framboidal pyrite grains. The samples from Seam-VI in the İbrice area have also similar distributions to those in the Şahin and Hasköy areas in the Malkara coalfield, while the contribution of woody peat-forming vegetation was relatively higher in the Pirinççeşme area (Figure 18). This plotting data also suggests that anoxic conditions were predominant and the contribution of woody peat-forming vegetation was high during peat accumulations of all working coal seams in the Malkara coalfield, which is also supported by palynofloral data from the study area (İslamoğlu et al., 2010).

The plotting data on the Tissue Preservation Index (TPI) *vs*. Gelification Index (GI) and Vegetation Index (VI) *vs*. Groundwater Index (GWI) also imply that the precursor peats of Seam-VI mainly accumulated under telmatic conditions, with occasional development of limno-telmatic conditions (Figure 19). The GI values of the samples could imply that the water table was not stable but constantly covered the peat surface (Figure 19a) (Kalaitzidis et al., 2004; Karayiğit et al., 2017; Omodeo-Salé et al., 2017). This assumption could be supported by the relatively low inertinite contents of the samples (Table 2). The previous palaeoclimate studies from the Danişmen Formation have also pointed out that humid climatic conditions were common during the Late Oligocene in the Thrace Basin (Akgün et al., 2013; Çelik et al., 2017; Suc et al., 2015). The existence of humid conditions and rich fungal assemblages during the Late Oligocene in the Thrace Basin could also have

caused the relatively funginite proportions of the samples. Similar observations have been reported in other coal mining areas in the Malkara coalfield and Yeniköy coalfield (Çelik et al., 2017; Karayiğit et al., 2021). Contrarily, the low GWI values of the studied samples and other coal seams in the Malkara coalfield might be indicators of drier conditions (Figure 19b). These low GWI values, on the other hand, could be expected from xylite-rich coals due to the masking effect of high telohuminite and low mineral matter contents (Kalaitzidis et al., 2004; Karayiğit et al., 2017; Oikonomopoulos et al., 2015; Životić et al., 2014). The TPI and VI values are higher than 1.0, suggesting that tissue preservation in the palaeomires was high due to anoxic conditions (Figure 19) (Kumar et al., 2024; Omodeo-Salé et al., 2017; Oskay et al., 2019; Zdravkov et al., 2017). These values also indicate that the contribution of woody vegetation was high during peat accumulation. In agreement, the palynoflora from the Malkara coalfield and other coal seams within the Danişmen Formation shows that coniferous peat-forming plants (e.g., Cupressaceae and Taxodioideae) were common vegetation elements during the Late Oligocene (Akgün et al., 2013; Çelik et al., 2017; İslamoğlu et al., 2010; Suc et al., 2015). Furthermore, *in-situ* fossilized wood trunks and root remains within the coal-bearing sequences were commonly reported from the study area and other coalfields in the Thrace basin (Çelik et al., 2017; Çevik-Üner et al., 2022; Karayiğit et al., 2022a). The previous studies on these remains also indicate the existence of coniferous peat-forming plants (e.g., *Glyptostroboxylon rudolphii* and *Taxodioxylon gypsaceum*) during the Late Oligocene (Akkemik, 2019; Akkemik and Sakınç, 2013; Çevik-Üner et al., 2022; Kayacık et al., 1995). Hence, the high TPI and VI values are expected for the İbrice area and other coal mining areas in the Malkara coalfield. Comparing the TPI and VI values of the studied samples from Seam-VI with those from other seams in the Şahin, Hasköy, and Pirinççeşme areas of the Malkara coalfield, the peat-forming vegetation and the degree of preservation of organic matter within the palaeomires of Seam-VI were presumably similar to those in the palaeomires of other seams in the Şahin and Hasköy areas. Hence, wet-forested and forested mires were commonly developed under the upper delta plain, and the contribution of herbaceous plants was increased due to the development

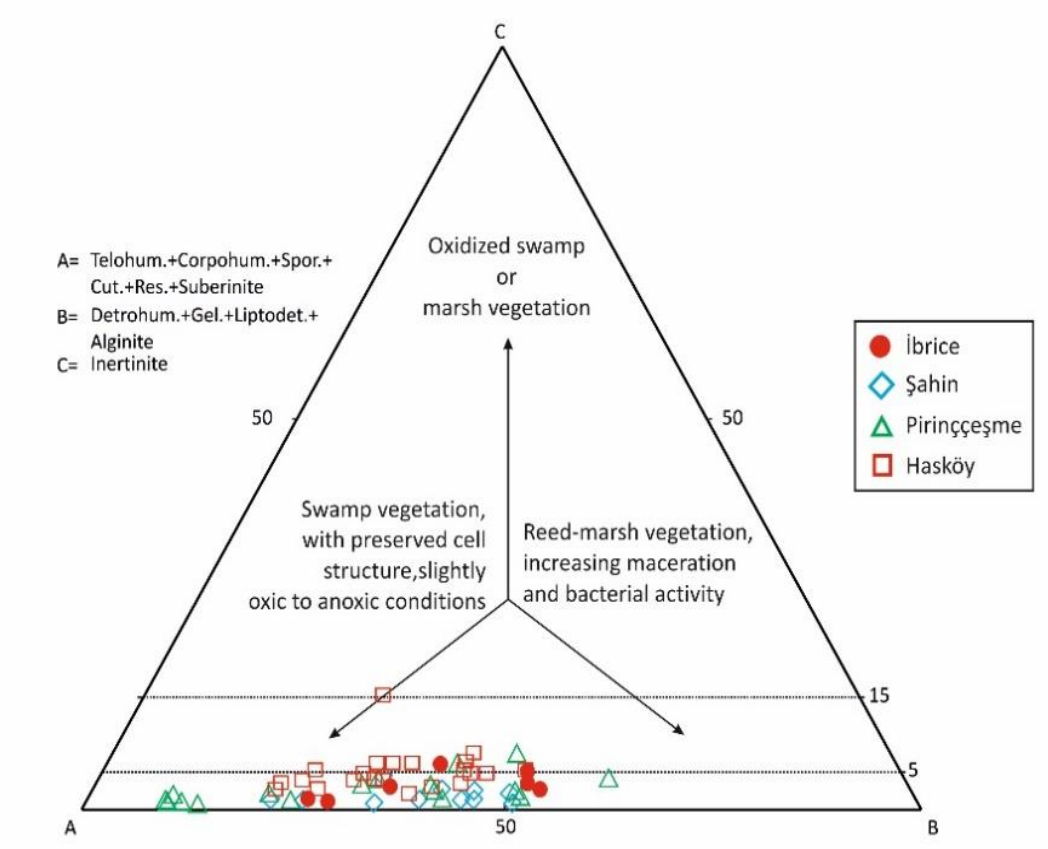

Figure 18: ABC ternary plot of the studied coal and samples from the Seam-VI in the İbrice area, and other coal seams in the Hasköy, Pirinççeşme and Şahin areas (after Mukhopadhyay, 1989; Hasköy, Pirinççeşme and Şahin areas data is from Karayiğit et al. (2022a).

Şekil 18: *İbrice sahasından incelenen Damar-VI ait kömür ve şeyl örnekleri ile Hasköy, Pirinççeşme ve Şahin sahalarından işletilen diğer damarlara ait verilerin ABC üçgen diyagramı üzerindeki dağılımları (Mukhopadhyay (1989)'a göre hesaplanmıştır; Hasköy, Pirinççeşme ve Şahin sahalarına ait veriler Karayiğit vd. (2022a)'dan alınmıştır).*

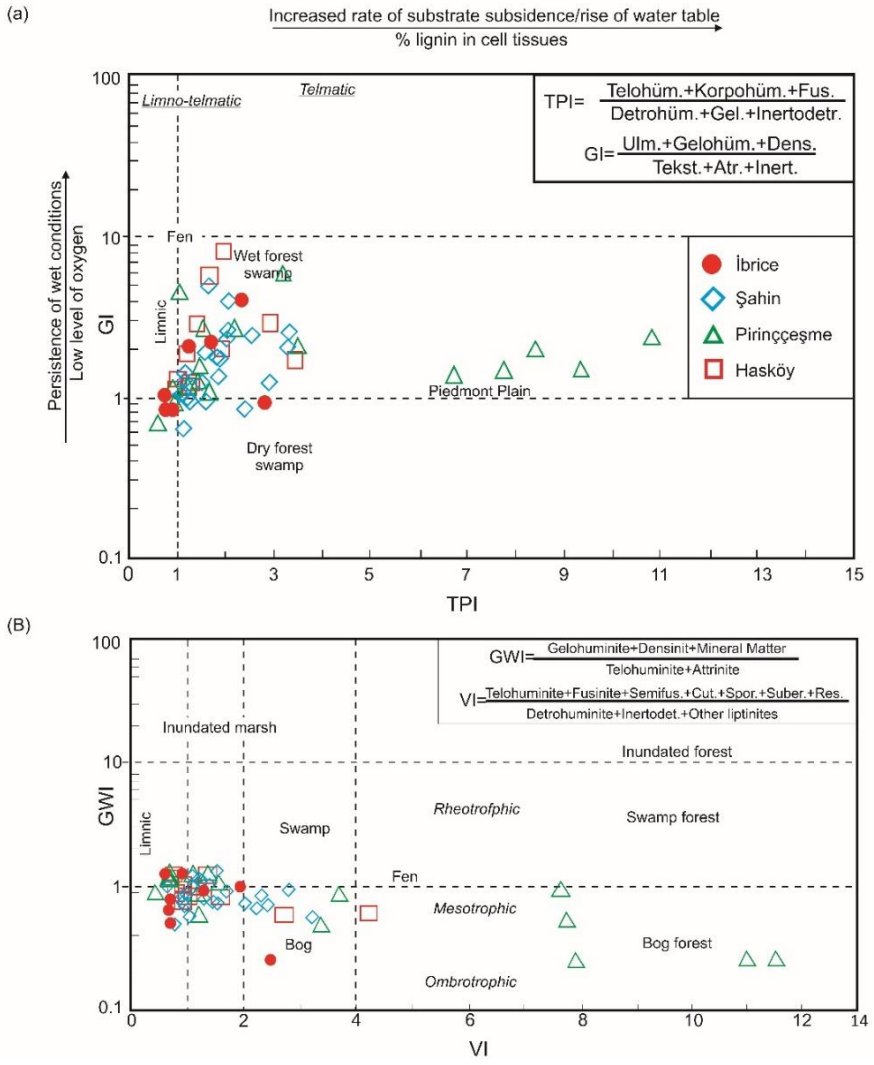

Figure 19: (a) GI *vs*. TPI plot of studied coal and samples from the Seam-VI in the İbrice area, and other coal seams in the Hasköy, Pirinççeşme and Şahin areas (after Diessel 1992, as modified by Kalaitzidis et al. 2004); b) VI *vs*. GWI plot of the studied coal and samples from the Seam-VI in the İbrice area, and other coal seams in the Hasköy, Pirinççeşme and Şahin areas (after Calder et al. 1991, as modified by Kalaitzidis et al. 2004; Hasköy, Pirinççeşme and Şahin areas data is from Karayiğit et al. (2022a).

Şekil 19: *İbrice sahasından incelenen Damar-VI ait kömür ve şeyl örnekleri ile Hasköy, Pirinççeşme ve Şahin sahalarından işletilen diğer damarlara ait verilerin (a) GI-TPI diyagramı üzerindeki dağılımları (Kalaitzidis vd. (2004) tarafından yapılan modifikasyona istinaden Diessel (1992)'ye göre hesaplanmıştır) ve (b) VI-GWI diyragamı üzerindeki dağılımları (Kalaitzidis vd. (2004) tarafından yapılan modifikasyona istinaden Calder vd. (1991)'e göre hesaplanmıştır) (Hasköy, Pirinççeşme ve Şahin sahalarına ait veriler Karayiğit vd. (2022a)'dan alınmıştır).*

of lower delta plain during the Late Oligocene in the study area (Karayiğit et al., 2022a; Omodeo-Salé et al., 2017; Oikonomopoulos et al., 2015). Besides, some significantly high TPI and VI values in the Pirinççeşme area could indicate that pure wet-forested mire was occasionally developed under upper delta plain conditions (Omodeo-Salé et al., 2017; Oikonomopoulos et al., 2015).

CONCLUSIONS

The results of this study revealed that the palaeomires of Seam-VI were mainly accumulated under telmatic conditions (forested mire), like other coal seams within the Danişmen Formation from the neighbouring Şahin, Hasköy, and Pirinççeşme areas in the Malkara coalfield; nevertheless, limno-telmatic conditions were occasionally developed. Under such conditions, the preservation of organic matter was high, and anoxic conditions were developed within palaeomires due to the high water table. Nevertheless, the presence of fossil shell remains and/or clay bands within xylite-rich lithotype coal samples and the existence of mineral-rich lithotype coal samples could indicate that sediment-laden water was introduced into palaeomires. Hence, ash yields, gross calorific values, and total C contents of samples are variable, and clay mineral aggregates were commonly observed during SEM studies. The sediment source area of clastic influx into palaeomires could have been mainly the Strandja and Rhodope massifs in the margins of the Thrace basin and/or formations bearing tuffite layers from the Late Eocene and Early Oligocene. Although the common presence of framboidal pyrite grains in the samples could be related to relatively low pH conditions within the palaeomires, their co-existence with syngenetic carbonate minerals (e.g., siderite and aragonite) and calcareous fossil shell remains could be evidence of very weak acidic to neutral conditions within the palaeomires.

Even though aluminosilicate minerals, particularly clay minerals, are abundant to dominant phases according to XRD whole-rock data, the majority of elemental enrichments in the Seam-VI seem to be mainly controlled by detritus accessory minerals in the samples. The clastic influx from the sulphide mineralization and ore deposits in the Strandja and Rhodope massifs into palaeomires seems to have caused the Co, Ni, Ge, and Mo enrichments due to the existence of accessory pentlandite and sphalerite grains within the clay mineral aggregates. The presence of siderite micronodules in the samples could indicate that Mn enrichments are related to these micronodules, and the source of Mn in the palaeomire could be dissolved surface water from Mn-bearing deposits in the Late Eocene-Early Oligocene sequences. The development of very weak acidic to neutral conditions might cause the formation of Mn-bearing siderite micronodules. The presence of Sr-bearing barite and (Ba,Sr)-sulphate overgrowths, which are related to alteration of feldspars and biotite grains within palaeomires, and syngenetic carbonate mineral bands could control the Sr enrichments in the samples. Overall, the clastic input ratio into palaeomires and pH conditions within these palaeomires seem to have elevated concentrations of the majority of enriched elements in Seam-VI.

ACKNOWLEDGEMENTS

A part of this study is supported by Scientific Research Projects Coordination Unit of Balıkesir University under the project number 2022/043. The authors would like to thank to Batı Trakya Madencilik Co. for permission sampling, Mr. Özgür Yüksel (Batı Trakya Madencilik Co.) and Dr. Cüneyt Bayraktaroğlu

(Atlı Enerji Co.) for their help during field study, and Ms. Yeşim A. Arslan (Standard Lab. Co.) for helps during XRF and ICP-OES analysis, and Prof. Dr. J. Hower for contributions. Finally, the authors would like thank Prof. Dr. Elif Varol-Muratçay, the editor-in-chief, Prof. Dr. Banu Koralay and the anonymous reviewer for their comments and corrections.

REFERENCES

Akgün F., Akkiraz, M.S., Üçbaş, S.D., Bozcu, M., Kapan-Yeşllyurt, S., Bozcu, A., 2013. Oligocene vegetation and climate characteristics in north-west Turkey: Data from the south-western part of the Thrace Basin. Turkish Journal of Earth Sciences, 22, 277-303. DOI: 10.3906/yer-1201-3

Akkemik Ü., Köse N., Poole, I., 2005. Sequoioideae (Cupressaceae) woods from the upper Oligocene of European Turkey (Thrace). Phytologia Balcanica, 11 (2), 119-131.

Altschuler, Z.S., Schnepfe, M.M., Silber, C.C., Simon, F.O., 1983. Sulfur diagenesis in Everglades peat and origin of pyrite in coal. Science, 221(4607), 221-227. DOI: 10.1126/science.221.4607.221

American Society for Testing and Materials (ASTM) D3174, 2020. Standard method of ash in the analysis sample of coal and coke from coal. ASTM, Philadelphia, 6pp. DOI: 10.1520/D3174-12R18

American Society for Testing and Materials (ASTM) D3175, 2020. Standard method of volatile matter in the analysis sample of coal and coke from coal. ASTM, Philadelphia, 14pp. DOI: 10.1520/D3175-20

American Society for Testing and Materials (ASTM) D3302/D3302M, 2022. Standard test method for total moisture in coal. ASTM, Philadelphia, 10pp. DOI: 10.1520/D3302_D3302M-22

American Society for Testing and Materials (ASTM) D4326, 2021. Standard test method for major and minor elements in coal ash by x-ray fluorescence. ASTM, Philadelphia, 9pp. DOI: 10.1520/D4326-21

American Society for Testing and Materials (ASTM) D5373, 2021. Standard Test Methods for determination of carbon, hydrogen and nitrogen in analysis samples of coal and carbon in analysis samples of coal and coke. ASTM, Philadelphia, 11pp. DOI: 10.1520/D5373-21

American Society for Testing and Materials (ASTM) D5865/D5865M, 2019. Standard test method for gross calorific value of coal and coke. ASTM, Philadelphia, 19pp. DOI: 10.1520/D5865_D5865M-19

Antoshkina, A.I., Ryabinkina, N.N., Valyaeva, O.V., 2017. Genesis of siderite nodules from the lower Carboniferous terrigenous sequence in the Subpolar Urals. Lithology and Mineral Resources, 52, 111-124. DOI: 10.1134/S0024490217020031

Bechtel, A., Markic, M., Sachsenhofer, R.F., Jelen B., Gratzer, R., Lücke, A., Püttmann, W., 2004. Paleoenvironment of the upper Oligocene Trbovlje coal seam (Slovenia). International Journal of Coal Geology, 57(1), 23-48. DOI: 10.1016/j.coal.2003.08.005

Bernstein, L.R., 1985. Germanium geochemistry and mineralogy. Geochimica et Cosmochimica Acta 49(11), 2409-2422. DOI: 10.1016/0016-7037(85)90241-8

Bohor, B.F., Triplehorn, D.M., 1993. Tonsteins: Altered volcanic-ash layers in coal-bearing sequences. GSA Special Papers, 285, 1-44.

Calder, J., Gibling, M., Mukhopadhyay, P., 1991. Peat formation in a Westphalian B piedmont setting, Cumberland Basin, Nova Scotia. Bulletin de la Societe geologique de France, 162(2), 238-298.

Chou, C.-L., 2012. Sulfur in coals: A review of geochemistry and origins. International Journal of Coal Geology, 100, 1-13. DOI: 10.1016/j.coal.2012.05.009

Crosdale, P.J., 1993. Coal maceral ratios as indicators of environment of deposition: do they work for ombrogenous mires? An example from the Miocene of New Zealand. Organic Geochemistry, 20, 797-809. DOI: 10.1016/0146-6380(93)90064-I

Çelik, Y., Karayiğit, A.I., Oskay, R.G., Kayseri-Özer, M.S., Christanis, K., Hower, J.C., Querol, X., 2021. A multidisciplinary study and palaeoenvironmental interpretation of middle Miocene Keles lignite (Harmancık Basin, NW Turkey), with emphasis on syngenetic zeolite formation. International Journal of Coal Geology, 237, Article Number 103691.

Çelik, Y., Karayiğit, A.İ., Querol, X., Oskay, R.G., Mastalerz, M., Kayseri-Özer, M.S., 2017. Coal characteristics, palynology, and palaeoenvironmental interpretation of the Yeniköy coal of late Oligocene age in the Thrace Basin (NW Turkey). International Journal of Coal Geology, 181, 103-123. DOI: 10.1016/j.coal.2021.103691

Çevik-Üner, B., Yılmaz-Şahin, S., Akkemik, Ü., 2022. Mineralogical and paleobotanical investigations of Oligo-Miocene petrified wood from the southwest of Thrace Basin (NW Turkey). Turkish Journal of Earth Sciences, 24, 383-397. DOI: 10.3906/yer-2106-2

Dai, S., Finkelman, R.B., 2018. Coal as a promising source of critical elements: Progress and future prospects. International Journal of Coal Geology, 186, 155-164. DOI: 10.1016/j.coal.2017.06.005

Dai, S., , Bechtel, A., Eble, C.F., Flore, R.M., French, D., Graham, I.T., Hood, M.M., Hower, J.C., Korasidis, V.A., Moore, T.A, Püttmann, W., Wei, Q., Zhao, L., O'Keefe, J.M.K., 2020a. Recognition of peat depositional environments in coal: A review. International Journal of Coal Geology, 219, Article number 103383. DOI: 10.1016/j.coal.2019.103383

Dai, S., Finkelman, R.B., French, D., Hower, J.C., Graham, I.T., Zhao, F., 2021. Modes of occurrence of elements in coal: A critical evaluation. Earth Science Reviews, 222, Article number 103815. DOI: 10.1016/j.earscirev.2021.103815

Dai, S., Finkelman, R.B., Hower, J.C., French, D., Graham, I.T., Zhao, L., 2023. Inorganic geochemistry of coal. Elsevier, Amsterdam, 438pp.

Dai, S., Hower, J.C., Finkelman, R.B., Graham, I.T., French, D., Ward, C.R., Eskenazy, G., Wei, Q., Zhao, L., 2020b. Organic associations of non-mineral elements in coal: A review. International Journal of Coal Geology, 218, 103347. DOI: 10.1016/j.coal.2019.103347

Dai, S., Seredin, V.V., Ward, C.R., Hower, J.C., Xing, Y., Zhang, W., Song, W., Wang, P., 2015. Enrichment of U–Se–Mo–Re–V in coals preserved within marine carbonate successions: geochemical and mineralogical data from the late Permian

Guiding Coalfield, Guizhou, China. Mineralium Deposita, 50, 159-186. DOI: 10.1007/s00126-014-0528-1

Dai, S., Ward, C.R., Graham, I.T., French, D., Hower, J.C., Zhao, L., Wang, X., 2017. Altered volcanic ashes in coal and coal-bearing sequences: A review of their nature and significance. Earth-Science Reviews, 175, 44-74. DOI: 10.1016/j.earscirev.2017.10.00

Dawson, G.K.W., Golding, S.D., Esterle, J.S., Massarotto, P., 2012. Occurrence of minerals within fractures and matrix of selected Bowen and Ruhr Basin coals. International Journal of Coal Geology, 94, 150-160. DOI: 10.1016/j.coal.2012.01.004

Demirtaş F., Bozcu, M., Koşun, E., Akkiraz, M.S., 2015. Petrography and palynology of late Oligocene and middle Miocene coals in the Gelibolu peninsula, NW Turkey. Turkish Journal of Earth Sciences, 24(4), 383-397. DOI: 10.3906/yer-1411-9

Diessel, C.F.K., 1992. Coal-bearing depositional systems, Springer, Berlin, 721pp.

Economic Commission for Europe-United Nations (E.C.E.-U.N.), 1998. International classification of in-seam coals. ECE, Geneva.

Ediger, V.Ş., 1981. Fossil fungal and algal bodies from Thrace Basin, Turkey. Palaeontographica Abteilung B, 179, 87-102.

Ediger, V.Ş., Alişan, C., 1989. Tertiary fungal and algal palynomorph biostratigraphy of the northern Thrace basin, Turkey. Review of Palaeobotany and Palynology, 58, 139-161. DOI: 10.1016/0034-6667(89)90082-1

Elsik, W.C., Ediger, V.Ş., Batı, Z., 1990. Fossil Fungal spore: Anatolinites gen. nov. Palynology, 14, 91-103. DOI: 10.1080/01916122.1990.9989374

Eminagaoglu, M., Oskay, R.G., Karayiğit, A.I., 2022. Evaluation of elemental affinities in coal using agglomerative hierarchical clustering algorithm: A case study in a thick and mineable coal seam (kM2) from Soma Basin (W. Turkey). International Journal of Coal Geology, 259, Article Number 104045. DOI: 10.1016/j.coal.2022.104045

Erarslan, C., Örgün, Y., 2017. Mineralogical and geochemical characterization of the Saray and Pınarhisar coals, Northwest Thrace Basin, Turkey. International Journal of Coal Geology, 173, 9-25. DOI: 10.1016/j.coal.2017.01.015

Erarslan, C., Örgün, Y., Balcı, N., 2020. Source and distribution of pyrite and inorganic sulfur isotopes in the Saray and Pınarhisar Coalfields, North Thrace Basin, Turkey. International Journal of Coal Geology, 227, 103533. DOI: 10.1016/j.coal.2020.103533

Erarslan, C., Örgün, Y., Bozkurtoğlu, E., 2014. Geochemistry of trace elements in the Keşan coal and its effect on the physicochemical features of ground- and surface waters in the coal fields, Edirne, Thrace Region, Turkey. International Journal of Coal Geology, 133, 1-12. DOI: 10.1016/j.coal.2014.09.003

Eskanazy, G., Finkelman, R.B., Chattarjee, S., 2010. Some considerations concerning the use of correlation coefficients and cluster analysis in interpreting coal geochemistry data. International Journal of Coal Geology, 83, 491-493. DOI: 10.1016/j.coal.2010.05.006

Fabiańska, M.J., Kurkiewicz, S., 2013. Biomarkers, aromatic hydrocarbons and polar compounds in the Neogene lignites

and gangue sediments of the Konin and Turoszów Brown Coal Basins (Poland). International Journal of Coal Geology, 107, 24-44. DOI: 10.1016/j.coal.2012.11.008

Finkelman, R.B., 1994. Modes of occurrence of potentially hazardous elements in coal: levels of confidence. Fuel Processing Technology, 39, 21-34. DOI: 10.1016/0378-3820(94)90169-4

Finkelman, R.B., Dai, S., French, D., 2019. The importance of minerals in coal as the hosts of chemical elements: A review. International Journal of Coal Geology, 212, Article number 103251. DOI: 10.1016/j.coal.2019.103251

Finkelman, R.B., Orem, W., Castranova, V., Tatu, C.A., Belkin, H.E., Zheng, B.S., Lerch, H.E., Maharaj, S.V., Bates, A.L., 2002. Health impacts of coal and coal use: possible solutions. International Journal of Coal Geology, 50, 425-443. DOI: 10.1016/S0166-5162(02)00125-8

Finkelman, R.B., Palmer, C.A., Wang, P., 2018. Quantification of the modes of occurrence of 42 elements in coal. International Journal of Coal Geology, 185, 138-160. DOI: 10.1016/j.coal.2017.09.005

Goodarzi, F., Swaine, D.J., 1994. The influence of geological factors on the concentration of boron in Australian and Canadian coals. Chemical Geology,118(1-4), 301-318. DOI: 10.1016/0009-2541(94)90183-X

Güllüdağ, C.B., Altunsoy, M., 2022. Major and trace element geochemistry of the Malkara (Tekirdağ, Turkeu) coals. Kütahya Dumlupınar University Institute of Graduate Studies, 51, 1-25.

Gültekin, A.H., 1998. Geochemistry and Origin of the Oligocene Binkılıç manganese deposit, Thrace Basin, Turkey. Turkish Journal of Earth Sciences, 7(1), 11-24.

Gültekin, A.H., 1999. Geology, mineralogy and geochemistry of the Cu-Mo deposit associated with the Şükrüpaşa intrusion, Dereköy, Kırklareli. Geological Bulletin of Turkey, 42(1), 29-45.

Gültekin, A.H., Balci, N., 2018. Geochemical Characteristics of Sedimentary Manganese Deposit of Binkılıç, Thrace Basin, Turkey. Journal of Geology and Geophysics, 7(3), Article Number 1000336. DOI: 10.4172/2381-8719.1000336

Gürdal, G., 2011. Abundances and modes of occurrence of trace elements in the Çan coals (Miocene), Çanakkale-Turkey. International Journal of Coal Geology, 87, 157-173. DOI: 10.1016/j.coal.2011.06.008

Gürgey, K., Batı, Z., 2018. Palynological and petroleum geochemical assessment of the lower Oligocene Mezardere Formation, Thrace Basin, NW Turkey. Turkish Journal of Earth Sciences, 27, 349-383. DOI: 10.3906/yer-1710-24

Hower, J.C., Clack, H.L., Hood, M.M., Hopps, S.G., Thomas, G.H., 2017. Impact of coal source changes on mercury content in fly ash: Examples from a Kentucky power plant. International Journal of Coal Geology, 170, 2-6. DOI: 10.1016/j.coal.2016.10.007

Hower, J.C., Eble, C., Johnston, M.N., Ruppert, L.R., Hopps, S.D., Margan, T.D., 2023. Geochemistry of the Leatherwood coal in eastern Kentucky with an emphasis on enrichment and modes of occurrence of rare earth elements. International Journal of Coal Geology, 280, Article Number 104387. DOI: 10.1016/j.coal.2023.104387

Hower, J.C., Ruppert, L.F., Williams, D.A., 2002. Controls on boron and germanium distribution in the low-sulfur Amos coal bed, Western Kentucky coalfield, USA. International Journal of Coal Geology, 53(1), 27-42. DOI: 10.1016/S0166-5162(02)00151-9

Huvaz, O., Karahanoglu, N., Ediger, V., 2007. The thermal gradient history of the Thrace basin, NW Turkey: Correlation with basin evolution processes. Journal of Petroleum Geology, 30, 3-24. DOI: 10.1111/j.1747-5457.2007.00003.x

International Committee for Coal Petrology (ICCP), 1993. International Handbook of Coal Petrography. Centre National de la Recherche Scientifique, Paris, 146pp.

International Committee for Coal Petrology (ICCP), 2001. The new inertinite classification (ICCP System 1994). Fuel, 80, 459-471. DOI: 10.1016/S0016-2361(00)00102-2

International Standard Organisation (ISO) 11760, 2005. Classification of coals. International Organization for Standardization, Geneva, 18pp.

International Standard Organisation (ISO) 11885, 2007. Determination of selected elements by inductively coupled plasma optical emission spectrometry (ICP-OES). International Organization for Standardization, Geneva, 38pp.

International Standard Organization (ISO) 7404–2, 2009. Methods for the petrographic analysis of coals -Part 2: Methods of Preparing Coal Samples. International Organization for Standardization, Geneva, 24pp.

İslamoğlu, Y., Harzhauser, M., Gross, M., Jiménez-Moreno, G., Coric, S., Kroh, A., Rögl, F., van der Made, J., 2010. From Tethys to Eastern Paratethys: Oligocene depositional environments, paleoecology and paleobiogeography of the Thrace Basin (NW Turkey). International Journal of Earth Sciences, 99, 183-200. DOI: 10.1007/s00531-008-0378-0

Kalaitzidis, S., Bouzinos, A., Papazisimou, S., Christanis, K., 2004. A short-term establishment of forest fen habitat during Pliocene lignite formation in the Ptolemais Basin, NW Macedonia. Greece. International Journal of Coal Geology, 57, 243-263. DOI: 10.1016/j.coal.2003.12.002

Karayiğit, A.I., Atalay, M., Oskay, R.G., Córdoba, P., Querol, X., Bulut, Y., 2020. Variations in elemental and mineralogical compositions of Late Oligocene, Early and Middle Miocene coal seams in the Kale-Tavas Molasse sub-basin, SW Turkey. International Journal of Coal Geology, 218, Article Number 103366. DOI: 10.1016/j.coal.2019.103366

Karayiğit, A.I., Azeri, N., Oskay, R.G., Hower, J.C., 2022c. Zeolite and associated mineral occurrences in high-sulphur coals from the middle Miocene upper coal seam from underground mines in the Çayirhan coalfield, (Beypazarı, Central Turkey). International Journal of Coal Geology, 256, Article Number 104010. DOI: 10.1016/j.coal.2022.104010

Karayiğit, A.İ., Cicioğlu Sütcü, E., Temel, A., Gündoğdu, M.N., 2022b. Vertical variations of minerals in clayey sedimentary rocks in the cores of two-deep exploration wells from the Kozlu coalfield (Zonguldak, NW Türkiye), with emphasis on tonstein (schieferton) formation. Turkish Journal of Earth Sciences, 31(6), 597-621. DOI: 10.55730/1300-0985.1822

Karayiğit, A.I., Gayer, R.A., Querol, X., Onacak, T., 2000. Contents of major and trace elements in feed coals from Turkish coal-fired power plants. International Journal of Coal Geology, 44, 169-184. DOI: 10.1016/S0166-5162(00)00009-4

Karayiğit, A.İ., Littke, R., Querol, X., Jones, T., Oskay, R.G., Christanis, K., 2017. The Miocene coal seams in the Soma Basin (W. Turkey): Insights from coal petrography, mineralogy and geochemistry. International Journal of Coal Geology, 173, 110-128. DOI: 10.1016/j.coal.2020.103624

Karayiğit, A.İ., Oskay, R.G., Çelik, Y., 2022a. Mineralogy, petrography, and Rock-Eval pyrolysis of late Oligocene coal seams in the Malkara coal field from the Thrace Basin (NW Turkey). International Journal of Coal Geology, 244, 103814. DOI: 10.1016/j.coal.2021.103814

Karayiğit, A.İ., Yiğitler, Ö., İşerli, S., Querol, X., Mastalerz, M., Oskay, R.G., Hower, J.C., 2019. Mineralogy and Geochemistry of Feed Coals and Combustion Residues from Tunçbilekand Seyitömer Coal-Fired Power Plants in Western Turkey. Coal Combustion and Gasification Products, 11, 18-31. DOI: 0.4177/CCGP-D-18-00011.1

Karayiğit, A.I., Yerin, Ü.O., Oskay, R.G., Bulut, Y., Córdoba, P., 2021. Enrichment and distribution of elements in the middle Miocene coal seams in the Orhaneli coalfield (NW Turkey). International Journal of Coal Geology, 247, Article Number 103854. DOI: 10.1016/j.coal.2021.103854

Kayacık, H., Aytuğ, B., Yaltırık, F., Şanlı, İ., Efe, A., Akkemik, Ü, İnan, M., 1995. Sequoiadendron giganteum trees lived near İstanbul in Late Tertiary. Journal of the Faculty of Forestry Istanbul University, 45, 15-22 (in Turkish with extended English summary).

Ketris, M.P., Yudovich, Ya.E., 2009. Estimations of Clarkes for Carbonaceous biolithes: World averages for trace element contents in black shales and coals. International Journal of Coal Geology, 78, 135-148. DOI: 10.1016/j.coal.2009.01.002

Kolcon, I., Sachsenhofer, R.F., 1999. Petrography, palynology and depositional environments of the early Miocene Oberdorf lignite seam (Styrian Basin, Austria). International Journal of Coal Geology, 41, 275-30. DOI: 10.1016/S0166-5162(99)00023-3

Kortenski, J., 1992. Carbonate minerals in Bulgarian coals with different degrees of coalification. International Journal of Coal Geology, 20, 225-242. DOI: 10.1016/0166-5162(92)90015-O

Kumar, A., K. Singh, A., Christanis, K., 2024. Paleodepositional environment and hydrocarbon generation potential of the Paleogene lignite in the Barmer Basin, Rajasthan, India. Journal of Asian Earth Sciences, 259, Article Number 105892. DOI: 10.1016/j.jseaes.2023.105892

Lebküchner, R.F., 1974. Beitrag zur kenntnis der geologie des Oligozans von Mittelthrakien (Türkei). Bulletin of the Mineral Research and Exploration, 83, 1-59.

Marcano, M. C., Frank, T. D., Mukasa, S. B., Lohmann, K. C., Taviani, M. 2015. Diagenetic incorporation of Sr into aragonitic bivalve shells: implications for chronostratigraphic and palaeoenvironmental interpretations. Depositional Record, 1, 38-52. DOI: 10.1002/dep2.3

Marchev, P., Singer, B.S., Jelev, D., Hasson, S., Moritz, R., Bonev, N., 2004. The Ada Tepe deposit: A sediment-hosted, detachment fault-controlled, low-sulfidation gold deposit in the Eastern Rhodopes, SE Bulgaria. Schweizerische Mineralogische und Petrographische Mitteilungen, 84(1-2), 59-78.

Mavrogonatos, C., Voudouris, P., Spry, P.G., Melfos V., Klemme S., Berndt J., Baker T., Moritz R., Bissig, T., Monecke, T., Zaccarini, F., 2018. Mineralogical study of the advanced argillic alteration zone at the konos hill Mo–Cu–Re–Au porphyry prospect, NE Greece. Minerals, 8(11), Article Number 479. DOI: 10.3390/min8110479

Melcher, F., Oberthür, T., Rammlmair, D., 2006. Geochemical and mineralogical distribution of germanium in the Khusib Springs Cu–Zn–Pb–Ag sulfide deposit, Otavi Mountain Land, Namibia. Ore Geology Reviews, 28(1), 32-56. DOI: 10.1016/j.oregeorev.2005.04.006

Moritz, R., Noverraz, C., Márton, I., Marchev, P., Spikings, R., Fontignie, D., Spangenberg, J.E., Vennemann, T., Kolev, K., Hasson, S., 2014. Sedimentary-rock-hosted epithermal systems of the Tertiary Eastern Rhodopes, Bulgaria: New constraints from the Stremtsi gold prospect. Geological Society Special Publication, 402(1), 207-230. DOI: 10.1144/SP402.7

Mozley, P.S., 1989. Relation between depositional environment and the elemental composition of early diagenetic siderite. Geology, 17, 704-706. DOI: 10.1130/0091-7613(1989)017<0704:RBDEAT>2.3.CO;2

Mukhopadhyay, P., 1989. Organic petrography and organic geochemistry of Tertiary coals from Texas in relation to depositional environment and hydrocarbon generation. Bureau of Economic Geology, Texas.

Nadkarni, R.A., 1980. Multitechnique multielemental analysis of coal and fly ash. Analytical Chemistry, 52(6), 929-935. DOI: 10.1021/ac50056a036

Oikonomopoulos, I.K., Kaouras, G., Tougiannidis, N., Ricken, W., Gurk, M., Antoniadis, P., 2015. The depositional conditions and the palaeoenvironment of the Achlada xylite-dominated lignite in western Makedonia. Greece. Palaeogeography, Palaeoclimatology, Palaeoecology, 440, 777-792. DOI: 10.1016/j.palaeo.2015.09.031

Okay, A.I., Özcan, E., Siyako, M., Bürkan, K.A., Kylander-Clark, A.R.C., Bidgood, M., Shaw, D., Simmons, M.D., 2023. Thrace Basin—An Oligocene Clastic Basin Formed During the Exhumation of the Rhodope Complex. Tectonics, 42(10), Article number e2023TC007766. DOI: 10.1029/2023TC007766

Ohta, E., Dogan, R., Batık, H., Abe, M., 1988. Geology and mineralization of Derekoy porphyry copper deposit, northern Thrace, Turkey. Bulletin of Geological Survey of Japan, 39(2), 115-134.

O'Keefe, J.M.K., Bechtel, A., Christanis, K., Dai, S., DiMichele, W.A., Eble, C.F., Esterle, J.S., Mastalerz, M., Raymond, A.L., Valentim, B.V., Wagner, N.J., Ward, R., Hower, J.C., 2013. On the fundamental difference between coal rank and coal type. International Journal of Coal Geology, 118, 58-87. DOI: 10.1016/j.coal.2013.08.007

Omodeo-Salé, S., Deschamps, R., Michel, P., Chauveau, B., Suarez-Ruiz, I., 2017. The

coal-bearing strata of the lower cretaceous Mannville Group (Western Canadian Sedimentary Basin, South Central Alberta), part 2: factors controlling the composition of organic matter accumulations. International Journal of Coal Geology, 179, 219-241. DOI: 10.1016/j.coal.2017.05.020

Oskay, R.G., Bechtel, A., Karayiğit, A.İ., 2019. Mineralogy, petrography and organic geochemistry of Miocene coal seams in the Kınık coalfield (Soma Basin-Western Turkey): Insights into depositional environment and palaeovegetation. International Journal of Coal Geology, 210, Article Number 103205. DOI: 10.1016/j.coal.2019.05.012

Oskay, R.G., Christanis, K., Inaner, H., Salman, M., Taka, M., 2016. Palaeoenvironmental reconstruction of the eastern part of the Karapınar-Ayrancı coal deposit (Central Turkey). International Journal of Coal Geology, 163, 100-111. DOI: 10.1016/j.coal.2016.06.022

Palmer, C.A., Tuncalı, E., Dennen, K.O., Coburn, T.C., Finkelman, R.B., 2004. Characterization of Turkish coals: a nationwide perspective. International Journal of Coal Geology, 60(2-4), 85-115. DOI: 10.1016/j.coal.2004.05.001

Pan, J., Nie, T., Vaziri Hassas, B., Rezaee, M., Wen, Z., Zhou, C., 2020. Recovery of rare earth elements from coal fly ash by integrated physical separation and acid leaching. Chemosphere, 248, Article number 126112. DOI: 10.1016/j.jece.2023.109921

Papanicolaou, C., Dehmer, J., Fowler, M., 2000. Petrological and organic geochemical characteristics of coal samples from Florina, lava, Moschopotamos and Kalavryta coal fields, Greece. International Journal of Coal Geology, 44, 267-292. DOI: 10.1016/S0166-5162(00)00014-8

Passey, S.R., 2014. The habit and origin of siderite spherules in the Eocene coal-bearing Prestfjall Formation, Faroe Islands. International Journal of Coal Geology, 122, 76-90. DOI: 10.1016/j.coal.2013.12.009

Perinçek, D., Ataş, N., Karatut, Ş., Erensoy, E., 2015. Geological factors controlling potential of lignite beds within the Danişmen formation in the Thrace Basin. Bulletin of the Mineral Research and Exploration, 150, 77-108. DOI: 10.19111/bmre.65462

Pickel, W., Kus, J., Flores, D., Kalaitzidis, S., Christanis, K., Cardott, B.J., Misz-Kennan, M., Rodrigues, S., Hentschel, A., Hamor-Vido, M., Crosdale, P., Wagner, N., ICCP, 2017. Classification of liptinite–ICCP system 1994. International Journal of Coal Geology, 169, 40-61. DOI: 10.1016/j.coal.2016.11.004

Querol, X., Cabrera, L., Pickel, W., López-Soler, A., Hagemann, H.W., Fernández-Turiel, J.L., 1996. Geological controls on the coal quality of the Mequinenza subbituminous coal deposit, northeast Spain. International Journal of Coal Geology, 29 (1-3), 67-91. DOI: 10.1016/0166-5162(95)00009-7

Querol, X., Chinchon, S., Lopez-Soler, A., 1989. Iron sulfide precipitation sequence in Albian coals from the Maestrazgo Basin, southeastern Iberian Range, northeastern Spain. International Journal of Coal Geology, 11(2), 171-189. DOI: 10.1016/0166-5162(89)90004-9

Querol, X., Whateley, M.K.G., Fernández-Turiel, J.L., Tuncali, E., 1997. Geological

controls on the mineralogy and geochemistry of the Beypazari lignite, central Anatolia, Turkey. International Journal of Coal Geology, 33(3), 255-271. DOI: 10.1016/S0166-5162(96)00044-4

Ruppert, L., Finkelman, R., Boti, E., Milosavljevic, M., Tewalt, S., Simon, N., Dulong, F., 1996. Origin and significance of high nickel and chromium concentrations in Pliocene lignite of the Kosovo Basin, Serbia. International Journal of Coal Geology, 29, 235-258. DOI: 10.1016/0166-5162(95)00031-3

Sakinç, M., Yaltirak, C., Oktay, F.Y., 1999. Palaeogeographical evolution of the Thrace Neogene Basin and the Tethys-Paratethys relations at northwestern Turkey (Thrace). Palaeogeography, Palaeoclimatology, Palaeoecology, 153(1-4), 17-40. DOI: 10.1016/S0031-0182(99)00071-1

Scott, A., 2002. Coal petrology and the origin of coal macerals: a way ahead? International Journal of Coal Geology, 50(1-4), 119-134. DOI: 10.1016/S0166-5162(02)00116-7

Shang, N., Liu, J., Han, Q., Jia, R., Zhao, S., 2023. Mineralogy and geochemistry of the Middle Jurassic coal from the Hexi Mine, Shenfu Mining Area, Ordos Basin: With an emphasis on genetic indications of siderite. International Journal of Coal Geology, 279, Article Number 104384. DOI: 10.1016/j.coal.2023.104384

Shen, M., Dai, S., French, D., Graham, I.T., Spiro, B.F., Wang, N., Tian, X., 2023. Geochemical and mineralogical evidence for the formation of siderite in Late Permian coal-bearing strata from western Guizhou, SW China. Chemical Geology, 637, Article Number 121675. DOI: 10.1016/j.chemgeo.2023.121675

Siyako, M., 2006. “Lignitic Sandstones" of The Trakya Basin. Bulletin of the Mineral Research and Exploration, 132, 63-72.

Spears, D.A., 2012. The origin of tonsteins, an overview, and links with seatearths, fireclays and fragmental clay rocks. International Journal of Coal Geology, 94, 22-31. DOI: 10.1016/j.coal.2011.09.008

Spiro, B.F., Liu, J., Dai, D., Zeng, R., Large, D., French, D., 2019. Marine derived $^{87}Sr/^{86}Sr$ in coal, a new key to geochronology and palaeoenvironment: Elucidation of the India-Eurasia and China-Indochina collisions in Yunnan, China. International Journal of Coal Geology, 215, Article 103304. DOI: 10.1016/j.coal.2019.103304

Suc J.-P., Gillet, H., Çağatay, M.N., Popescu, S.-M., Lericolais, G., Armijo, R., Melinte-Dobrinescu, M.C., Şen, Ş., Clauzon, G., Sakinç, M., Zabci, C., Ucarkus, G., 2015. The region of the Strandja Sill (North Turkey) and the Messinian events. Marine and Petroleum Geology, 66, 149-164. DOI: 10.1016/j.marpetgeo.2015.01.013

Sykes, R., Fowler, M.G., Pratt, K.C., 1994. A Plant Tissue Origin for Ulminites A and B in Saskatchewan Lignites and Implications for R_o. Energy and Fuels, 8(6), 1402–1416. DOI: 10.1021/ef00048a032

Sýkorová, I. Pickel, W., Christanis, K., Wolf, M., Taylor, G.H., Flores, D., 2005. Classification of huminite-ICCP system 1994. International Journal of Coal Geology, 62, 85-106. DOI: 10.1016/j.coal.2004.06.006

Şafak, Ü., 2019. Paleoenvironmental features and ostracod investigation of Paleogene-Neogene sequences in Babaeski-Lüleburgaz- Muratli-Çorlu region (southeastern Thrace, Turkey). Bulletin of

the Mineral Research and Exploration, 160, 45-79.

Taner, M.F., and Çağatay, A., 1983. Geology and mineralogy of the ore deposits of the Istranca Massif. Bulletin of the Geological Society of Turkey, 26, 31-40 (in Turkish with English abstract).

Tuncalı, E., Çiftci, B., Yavuz, N., Toprak, S., Köker, A., Gencer, Z., Ayçık, H., Pahin, N., 2002. Chemical and Technological Properties of Turkish Tertiary Coals. MTA Publication, Ankara, 401pp.

Tuncer, A., Karayiğit, A.İ., Oskay, R.G., Tunoğlu, C., Kayseri-Özer, M.S., Gümüş, B.A., Bulut, Y., Akbulut, A., 2023. A multi-proxy record of palaeoenvironmental and palaeoclimatic conditions during Plio-Pleistocene peat accumulation in the eastern flank of the Isparta Angle: A case study from the Şarkikaraağaç coalfield (Isparta, SW Central Anatolia). International Journal of Coal Geology, 256, Article Number 104149. DOI: 10.1016/j.coal.2022.104149

Turgut, S., Eseller, G., 2000. Sequence Stratigraphy/tectonics and depositional history in eastern Thrace Basin/ NW Turkey. Marine and Petroleum Geology, 17, 61-100. DOI: 10.1016/S0264-8172(99)00015-X

Xu, N., M. Peng, Q. Li, Xu, C., 2020. Towards consistent interpretations of coal geochemistry data on whole-coal versus ash bases through machine learning. Minerals, 10, Article Number 328. DOI: 10.3390/min10040328

Xu, N., Xu, C., Finkelman, R.B., Engle, M.A., Li, Q., Peng, M., He, L., Huang, B., Yang, Y., 2022. Coal elemental (compositional) data analysis with hierarchical clustering algorithms. International Journal of Coal Geology, 249, Article 103892. DOI: 10.1016/j.coal.2021.103892

Xu, N., Zhu, W., Wang, R., Li, Q., Wang, Z., Finkelman, R.B., 2023. Application of self-organizing maps to coal elemental data. International Journal of Coal Geology, 277, Article Number 104358. DOI: 10.1016/j.coal.2023.104358

Ward, C.R., 2002. Analysis and significance of mineral matter in coal seams. International Journal of Coal Geology, 50(1-4), 135-168. DOI: 10.1016/S0166-5162(02)00117-9

Ward, C.R., 2016. Analysis, origin and significance of mineral matter in coal: An updated review. International Journal of Coal Geology, 165, 1-27. DOI: 10.1016/j.coal.2016.07.014

Ward, C.R., Corcoran, J.F., Saxby, J.D., Read, H.W., 1996. Occurrence of phosphorus minerals in Australian coal seams. International Journal of Coal Geology, 30, 185-210. DOI: 10.1016/0166-5162(95)00055-0

Yang, Q., Zhang, X., Ulrich, T., Zhang, J., Wang, J., 2022. Trace element compositions of sulfides from Pb-Zn deposits in the Northeast Yunnan and northwest Guizhou Provinces, SW China: Insights from LA-ICP-MS analyses of sphalerite and pyrite. Ore Geology Reviews, 141, Article Number 104639. DOI: 10.1016/j.oregeorev.2021.104639

Yudovich, Ya.E., 2003. Notes on the marginal enrichment of Germanium in coal beds. International Journal of Coal Geology, 56(3-4), 223-232. DOI: 10.1016/j.coal.2003.08.003

Zdravkov, A., Bechtel, A., Sachsenhofer, R.F., Kortenski, J., 2017. Palaeoenvironmental

implications of coal formation in Dobrudzha Basin, Bulgaria: Insights from organic petrological and geochemical properties. International Journal of Coal Geology, 180, 1-17. DOI: 10.1016/j.coal.2017.07.004

Zdravkov, A., Stefanova, M., Worobiec, E., Bechtel, A., Marinov, S., Kortenski, J., 2020. Implications for peat formation in Maritsa-West Basin, SE Bulgaria: Insights from organic petrology, palynology and biomarker assemblage. International Journal of Coal Geology, 222, Article Number 103447. DOI: 10.1016/j.coal.2020.103447

Zieger, L., Littke, R., 2019. Bolsovian (Pennsylvanian) tropical peat depositional environments: The example of the Ruhr Basin, Germany. International Journal of Coal Geology, 211, Article Number 103209. DOI: 10.1016/j.coal.2019.103209

Životić, D., Bechtel, A., Sachsenhofer, R., Gratzer, R., Radić, D., Obradović, M., Stojanović, K., 2014. Petrological and organic geochemical properties of lignite from the Kolubara and Kostolac basins, Serbia: Implication on Grindability index. International Journal of Coal Geology, 131, 344-362. DOI: 10.1016/j.coal.2014.07.004